ADVANCED ENERGY & SUSTAINABILITY RESEARCH
Open Access
www.advenergysustres.com

Optimization Design and Application of Niobium-Based Materials in Electrochemical Energy Storage

*Yue Lian, Ning Yang, Dawei Wang, Yujing Zheng, Chaolei Ban, Jing Zhao, and Huaihao Zhang**

In various energy storage devices, the development and research of electrode materials has always been a key factor. Nb-based materials are one choice of energy storage materials because of the good ion-diffusion channels and high theoretical capacity. More importantly, their advantages, such as safe potential range, high structural stability, and highly reversible redox reaction with small strain, are conducive to efficient, safe, and stable energy storage development. Based on aforementioned superiority, much of the research is to further optimize performance of Nb-based materials by unique nano-morphology design, lattice regulation, and functional additives composition, showing good electrochemical performance in many kinds of devices. This review mainly introduces the classification of Nb-based materials used for energy storage, their application in different battery systems, and common optimization methods. Accordingly, the deficiencies and prospects of Nb-based materials are also discussed in detail.

1. Introduction

In the context of economic globalization, the excessive consumption of basic resources (such as coal, oil, natural gas, etc.) and the aggravation of environmental pollution have drawn more and more attention to renewable energy all over the world. However, the instability and poor sustainability of renewable resources make it difficult to be used directly. Therefore, the search for sustainable and efficient energy conversion and storage technologies, especially electrochemical energy storage devices such as lithium-ion battery (LIB),[1] sodium-ion battery (SIB),[2,3] lithium–sulfur battery (Li–S),[4] supercapacitor (SC),[5,6] is one of the development directions of new energy. Herein, the main difficulties in respect to energy storage equipment is to exploit efficient and stable electrode materials with sufficient electrochemical capacity.

In the early 19th century, the discovery of niobium (Nb) in ores initiated its study. Niobium has been used in metallurgical industry, mechanical industry, and electronics industry in the early stage.[7] In recent years, Nb-based materials as electrode materials in the field of electrochemical energy storage also caused a hotspot discussion.[8] Although graphite with a high specific capacity (theoretical capacity of 372 mAh g^{-1}), low cost, and long cycle life characteristics has been well used as conventional commerciallithium ion capacitor (LIC) materials, the serious safety problems still exist due to the electrolyte decomposition at low working potential (0.8 V vs Li/Li^+) and lithium dendrites formation (0.2 V vs Li/Li^-), which hinders its application.[9] In comparison, Nb-based materials, with the redox reactions within the safe potential range (1.0–2.0 V), have a high theoretical capacitance (even higher than graphite[10]) and have attracted more attention and research for its good prospects.

In fact, the quantity of research articles about Nb-based materials in electrochemical energy storage has increased significantly (**Figure 1**), and most of them have achieved high performance improvement, especially Nb_2O_5[11] and niobium titanium oxide ($Ti_2Nb_{2x}O_{4+5x}$).[12] In this article, the composition of niobium-based materials, main modification methods and applications in different systems are summarized. Also, the potential bottlenecks and prospects are briefly discussed.

Dr. Y. Lian, N. Yang, Dr. D. Wang, Y. Zheng, J. Zhao, Prof. H. Zhang
School of Chemistry and Chemical Engineering
Yangzhou University
Yangzhou 225002, P. R. China
E-mail: hhzhang@yzu.edu.cn

C. Ban
School of Materials Science and Technology
Liaocheng University
Liaocheng 252059, P. R. China

The ORCID identification number(s) for the author(s) of this article can be found under https://doi.org/10.1002/aesr.202000038.

DOI: 10.1002/aesr.202000038

2. Nb-Based Materials

The research of Nb-based materials in energy storage has been made much progress, including niobium oxide, niobium sulfide, niobium carbon/nitride and its polyoxides.

2.1. Niobium Oxide

Niobium has a series of distinct valence states (Nb^{2+}, Nb^{3+}, Nb^{4+}, and Nb^{5+}) corresponding to a variety of niobium oxide (NbO_x), involving NbO, Nb_2O_3, NbO_2, and Nb_2O_5. Most niobium oxides used for energy storage have good ion-transport channels

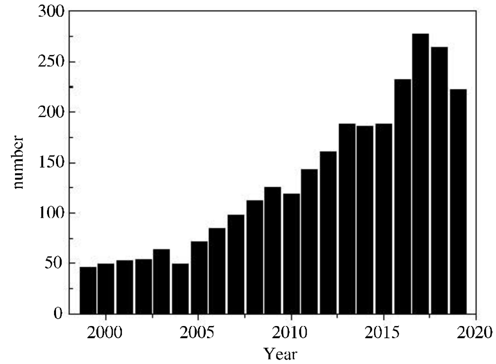

Figure 1. Quantity of SCI articles based on niobium. (From Web of Science by searching phrase "Nb" and "electrochemical").

and stable lattice structures, which are well adapted to the structural expansion and phase change caused by ion embedding. We collected some cell maps of niobium oxide (**Figure 2**) to facilitate understanding.

NbO, with plane-centered cubic crystal structure, is the minimum valent oxide in niobium oxide system. Its Oh space group is 3 Nb atoms at the site 3(c) (0 1/2 1/2; 1/2 0 1/2; 1/2 1/2 0) and 3 O atoms at the site 3(d) (1/2 0 0; 0 1/2 0; 0 0 1/2), along with typical metal electrical behavior with resistivity about 20 μΩ cm^{-1}.[13] NbO, with lower thermal stability than that of Nb_2O_5, can be converted into pentavalent niobium under oxygen environment in the range of 300–500 °C.[14] Although few researches on NbO, its application in energy storage system has been reported. Zhou[15] successfully synthesized NbO electrode material using Nb and Nb_2O_5 as raw materials by high-temperature solid-phase method, and analyzed its energy storage mechanism via in situ X-ray diffraction (XRD) and a series of non-in situ characterization. The redox peaks of NbO were located at 1.5 and 1.9 V, respectively, corresponding to $x\text{Li}^- + xe^- + \text{NbO} \Leftrightarrow \text{Li}_x\text{NbO}$. Under the influence of embedded lithium, the lattice structure of NbO will undergo a weak expansion (from 0.42083 nm to 0.42122 nm), but the cycle test proves the energy storage mechanism with high reversibility.

From Figure 2, NbO_2 has various crystal structure. Among them, tetragonal NbO_2 (MP-557057) has been reported as LIC energy storage material. NbO_2 has resistivity ≈104 Ω cm^{-1} at room temperature, theoretical capacity 429 mAh g^{-1} and low lithium embedding/disembedding potential 1.3 V/1.4 V.[16] Jeong[17] used NbO_2 particles deposited in carbon-based materials as LIC cathode materials and investigated the lithium storage mechanism. The reduction peak at 1.5–1.75 V and the oxidation peak at 1.0–1.2 V/1.8 V match to $x\text{Li}^+ + xe^- + \text{NbO}_2 \Leftrightarrow \text{Li}_x\text{NbO}_2$. Meanwhile, in situ XRD results show that the volume change of NbO_2 is only 0.14% as lithium insertion, indicating its zero-strain active property (usually defined as the volume change ratio less than 1%) and the potential for highly stable LIC material. However, due to the poor conductivity, the observed capacity in this report is much lower than the theoretical capacity. Therefore, constructing appropriate conductive network can notably activate the electrochemical activity of NbO2 to improve its capacity utilization.

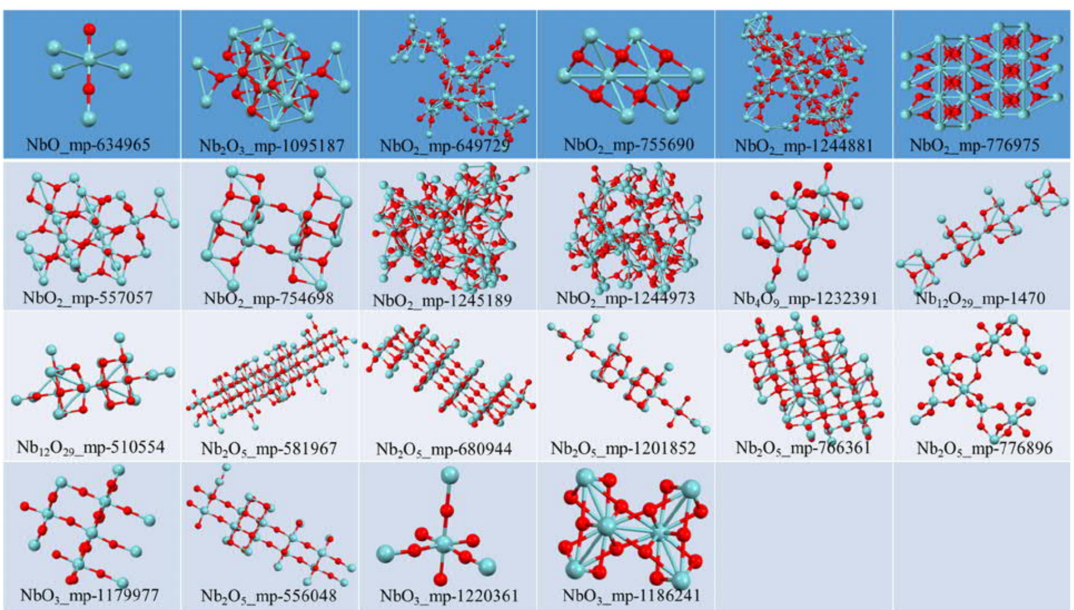

Figure 2. Partial niobium oxide cell diagram.

$Nb_{12}O_{29}$ (chemical formula $Nb_2^{4+}Nb_{10}^{5+}O_{29}$, similar to $Ti_2Nb_{10}O_{29}$) has two crystal structures, namely orthophase (O-) and monocline (M-). In local crystal structure, both crystals are composed of NbO_6 octahedral blocks with 4 × 3 shared angles of perovskite, but different in long-distance sequence,[18] which lead to their distinct properties. For example, M- is magnetic, while O- is not. The $4d^1$ electron (Nb^{4+}) endows $Nb_{12}O_{29}$ high electrical conductivity, three orders of magnitude higher than pure Nb^{5+}.[19] In addition, $Nb_{12}O_{29}$ has an open crystal structure derived from an A2/m space groups, which favors a large ions diffusion coefficient. Based on the aforementioned theoretical advantages, Lin and co-workers[20] reduced Nb_2O_5 using H_2/Ar at high temperature to prepare $Nb_{12}O_{29}$ micron particles (0.5–3 μm) for LIB. The successful synthesis of $Nb_{12}O_{29}$ (No. 73-1610) and the existence of Nb^{4+} (X-ray photoelectron spectroscopy [XPS]: 209.0 and 205.8 eV) and Nb^{5+} (XPS: 210.1 and 207.3 eV) were confirmed by XRD and XPS. The diffusion coefficient D of Li^+ also can be acquired using the linear fitting lines in the low frequency (electrochemical impedance spectroscopy [EIS]) according to the following equations

$$Z' = R_\Omega + R_{ct} + \sigma\omega^{-1/2} \quad (1)$$

$$D = R^2T^2/(2S^2F^4C^2\sigma^2) \quad (2)$$

where R, T, and F are the gas constant, absolute temperature, and Faraday constant, respectively; where S and C are the surface area of electrode and Li^+ concentration. σ is the curve slope belonging to the relation of Z' and $\omega^{-1/2}$ in low-frequency region based on equation. Compared with $Ti_2Nb_{10}O_{29}$, the large ion channels from big ion size of Nb^{4+} afford $Nb_{12}O_{29}$ a higher ion-diffusion coefficient ($5.42 \times 10^{-15}\,cm^2\,s^{-1}$). Similar to most Nb-based materials, its high safe working potential (≈1.69 V and ≈1.72 V) and high capacitance (287 mAh g^{-1}) make it a good application prospect in LIB. In summary, Nb^{4+} with uncoordinated electrons has favorable effects on electrical conductivity and ion transport channels of the material, thus promoting its electrochemical performance in LIB.

Nb_2O_5, the best-known niobium oxide, manifests itself as an n-type transition metal oxide semiconductor with a bandgap of about 3.4 eV.[21] Its excellent performance has been demonstrated in gas sensing, catalysis, electrochromic, and photoelectrode fields as well as energy storage anodes.[22] Depending on heat treatment conditions, Nb_2O_5 has a variety of crystal types, comprising pseudohexagonal (TT-Nb_2O_5), orthogonal (T-Nb_2O_5), tetragonal (M-Nb_2O_5), and monoclinic (H-Nb_2O_5).[23] Different crystal types have a great influence on its energy storage performance, among which T-Nb_2O_5 (MP-776896) shows the best energy storage property in existing reports.[24]

T-Nb_2O_5 consists of 6/7 O^{2+} surrounding Nb^{5+} to form the NbO_6 and NbO_7 polyhedra with shared edges/angles.[25] According to atoms arrangement, its crystal structure can be deemed as two alternating layers of atoms, namely loose 4 g-layer and denser 4 h-layer.[26] The former provides excellent storage and transmission sites for the embedded ions, and the interconnected open channel (0.39 nm) between NbO_x thin plates reduces the diffusion barrier and offers stable and effective tunnels for the embedded ions, without the limitation from the solid-state diffusion and volume expansion.[27] In terms of these advantages, there have been many reports on energy storage of T-Nb_2O_5. For example, Mai and co-workers[28] prepared egg-yolk microspheres (0.3–3 μm) using niobium oxalate and sucrose by spray-drying and annealing. According to the power law formula ($i = av^b$) and its derived formula, the energy storage mechanism is controlled by the fast ion-embedding/disembedding capacitive behavior. To be specific, assuming that the current obeys a power-law relationship with the scan rate, this leads to

$$i = av^b \quad (3)$$

where a and b are adjustable values. In particular, the b-value 0.5 represents a total diffusion-limited process, whereas 1 indicates a capacitive process.

From the Equation (3), the total capacitive contribution at a certain scan rate could be quantified by dividing the response current into two parts, current contribution from the capacitive-controlled process (k_1v, corresponding to $b = 1$) and diffusion-controlled process ($k_2v^{1/2}$, against $b = 0.5$), and therefore the Equation (3) can be converted into

$$i(V) = k_1v + k_2v^{1/2} \quad (4)$$

where k_1 and k_2 are constants at a fixed potential. For an analytical purpose, the Equation (4) can be rearranged slightly into

$$i(V)/v^{1/2} = k_1v^{1/2} + k_2 \quad (5)$$

Therefore, the value of k_1 is determined as the slope by plotting $i(V)/v^{1/2}$ versus $v^{1/2}$, and then the capacitive and diffusion contributions can be obtained. This report confirmed that T-Nb_2O_5 stores lithium mainly through intercalated pseudocapacitance ($Nb_2O_5 + xLi^+ + xe^- \Leftrightarrow Li_xNb_2O_5$) through in situ XRD and kinetic studies. Specifically, the diffraction peaks of the crystal plane (001) and (180) are slightly periodically shifted due to the embedding Li^+ in the energy storage process. Clearly, the crystal structure of T-Nb_2O_5 will not be damaged during the Li^+ embedding process and maintains good cyclic stability (retains 98% capacity after 1000 cycles). The excellent T-Nb_2O_5 lattice advantages (large lattice channel and fast transport dynamics) make it well studied and applied in various batteries (including $Li^+/Na^+/K^+$ system and polyvalent metal ion system) and SCs (**Figure** 3a–c).

Different from T-Nb_2O_5, most of the other Nb_2O_5 crystals are unconducive to energy storage on account of polyphase transformation and bad ion transfer. But for all this, continuous and fast ions diffusion channel of H-Nb_2O_5 still attracts attention. The anisotropy of electron and ion transport is the main cause of its asynchronous phase transition and real performance degradation.[14] To alleviate this problem, Zhang and co-workers[29] coated thin amorphous N-doped carbon layer on the surface of micron single-crystal H-Nb_2O_5 particles to prepare N-C@MSC- Nb_2O_5 composite materials (Figure 3d–i). The thin amorphous carbon layer eliminates the spatial and temporal unsynchronization of Li^+ (de) intercalation due to local inhomogeneity, effectively inhibiting the capacity attenuation by reason of the random phase transition of H-Nb_2O_5. Unlike interlayer insertion materials with phase transitions, the orientation of Li^+ diffusion channels in H-Nb_2O_5 is parallel to the expansion direction of the crystal structure, rather than perpendicular to each other. Both are responsible for its high stability (retaining

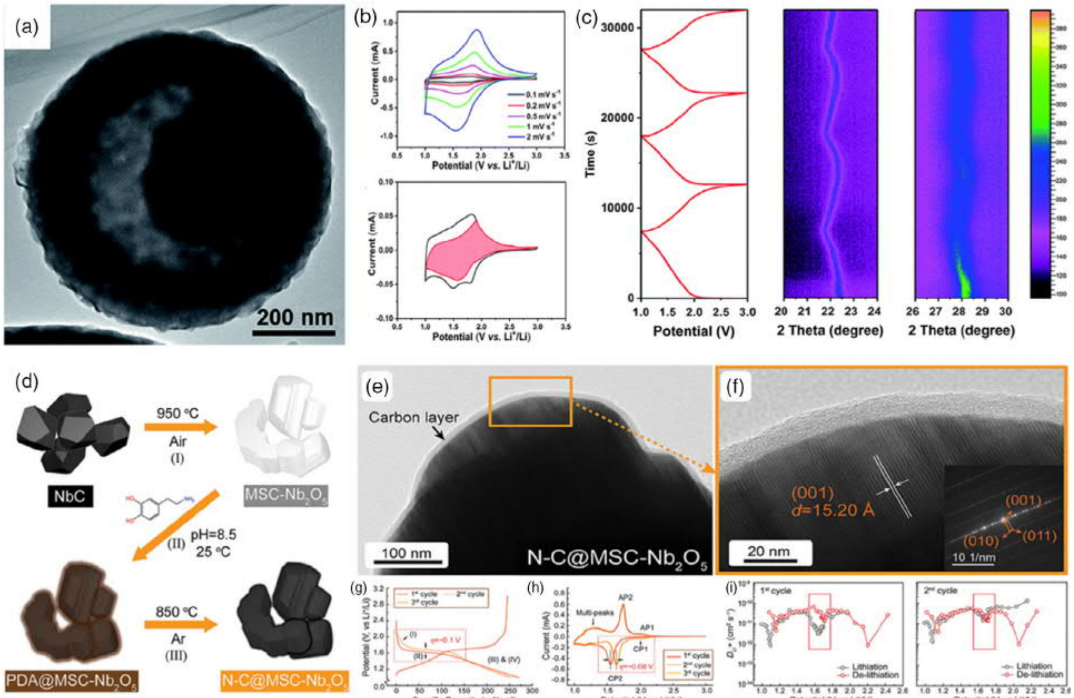

Figure 3. a) TEM, b) CV and c) In-situ XRD of T-Nb2O5;[28] d) Synthetic procedure, e–f) HRTEM, g) GCD, h) CV and i) chemical diffusion coefficients D_{Li^+} versus potential (vs Li^+/Li) plots of H-Nb_2O_5.[29] a–c) Reproduced with permission.[28] Copyright 2016, Royal Society of Chemistry. d–i) Reproduced with permission.[29] Copyright 2016, Wiley-VCH.

83% capacity after 1000 cycles). In addition, H-Nb_2O_5 good conductivity and transmission dynamics because of carbon layer will help increase its electric capacity (>250 mAh g^{-1} at 50 mA g^{-1}). In conclusion, in terms of the high capacity and structural stability of H-Nb_2O_5, the amorphous thin carbon layer is utilized to optimize the interface stability and the ion/electron transport uniformity, and to obstruct the adverse reaction between the energy storage subject and electrolyte. The resultant synchronous phase transition will have positive effects on the electrochemical performance of the inserted energy storage materials (**Figure 4**).

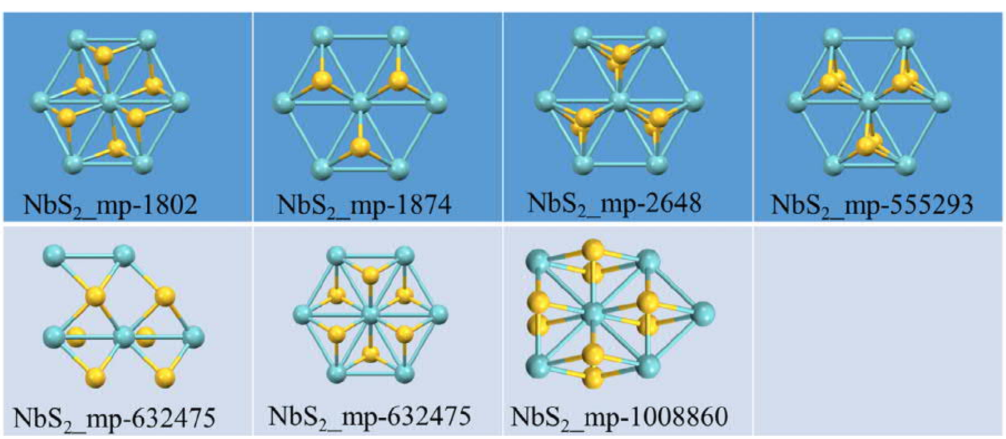

Figure 4. Partial NbS_2 cell diagram.

2.2. Niobiyl Sulfide

Similar to the oxide, niobiyl sulfide also has many sulfur compounds due to its polyvalent state, consisting of NbS, NbS_3, Nb_3S_4, Nb_3S_5, NbS_6, etc. However, NbS_2 has been reported many times in energy storage for its stability and electrochemical applicability.

As typical transition metal disulfide (TMDs, MX_2), NbS_2, a 2D layered material with a layer of metal atoms (Nb) sandwiched between two-layer sulfur atoms,[30] exhibits typical lamellae structure and resistivity (1.0×10^{-3} to $1.0 \times 10^{-4}\,\Omega\,cm^{-1}$) superior to that of most TMDs. Its unique covalent bonding layer and weak interlayer van der Waals force provide smooth 2D transport path and large ion-storage space for ions and electrons. Because of the S-Nb-S crystal structure with Nb plane sandwiched between two S plane layers, NbS_2 has direct bandgap, strong spin orbit coupling, and good electronic mechanical properties.[31] The high specific surface area and open layer structure of NbS_2 offer convenient atomic interface contact/interaction pathways for ions, along with its high theoretical capacity and relatively low operating potential, which make it a potential high-energy storage material.[32]

Although the aforementioned energy storage advantages, a series of problems of NbS_2 are also obvious. Because of the abundant functional groups on surface, its accumulation and agglomeration is easy to happen.[33] In addition, on account of uneven spacing and agglomeration, electrolyte is not easy to enter the internal space of material, which reduces the utilization ratio of NbS_2. Therefore, it is a common direction to adjust the layer spacing of lamellar structure. There have been many reports on the strategies of layer spacing regulation, such as cationic stripping, chemical stripping, wet ball grinding, ultrasonic stripping, and other physical methods. Yang and co-workers[30] adjusted the layers space of NbS_2 by chemical stripping and restacking, which can facilitate the increase in electron/Na ion diffusion coefficient and reduce volume change during the cycles. After reconstruction, the space between adjacent NbS_2 layers is 6.65 nm and each sheet consists of 14–15 monolayer with good phase structure. In situ XRD shows peak shift and its intensity decrease at 15°, corresponding to the lattice expansion as Na^+ embedding. A new peak representing Na_xNbS_2 appears at 13.5°, confirming the new phase structure generated by Na^+ embedding. At the lowest voltage (0.01 V), the main peak standing for NbS_2 almost disappears, while the new peak of Na_xNbS_2 is further strengthened. During the disembedding process, the peak changes are reversed and remain well periodic after multiple cycles, evidencing that the good reversibility of energy storage mechanism ($NbS_2 + xNa^+ + xe \Leftrightarrow Na_xNbS_2$) contributes to the cycling stability of the material.

Also as a sulfur compound, $NbSe_2$ is lamellar with crystal structure similar to NbS_2. Choi and co-workers[34] synthesized the less-layer $NbSe_2$@graphene heterostructure and studied the $NbSe_2$ phase-transition mechanism in Li^+ embedding/disembedding process. During the embedding one, $NbSe_2$ undergoes a phase transition from Li_xNbSe_2 to Li_2Se and Nb, whereas for the disembedding one, Li_2Se and Nb phases transform to $NbSe_2$ again. The cyclic stability of pure $NbSe_2$ in energy storage is necessarily unsatisfied due to the phase transitions.

In this report, less layer $NbSe_2$@graphene heterostructure (WBMNG) was prepared by wet ball grinding. Based on wet ball milling, $NbSe_2$ particles (200 nm transverse and 7.7 nm [37 layers] thick) were embedded into larger graphene (1 μm transverse and 1.7 nm [5 layers] thick). This heterostructure, with $NbSe_2$ particles embedding into large thin graphene sheets, not only prevents $NbSe_2$ aggregation but also results in the increase in the contact area between electrolyte and active material. Furthermore, thin graphene sheets supply efficient transfer paths for Li^+ and electrons, thereby effectively responding to the changes in current rates. In fact, it can achieve high reversible capacity of $\approx$1000 mAh g^{-1} in lithium half-cell, and maintain $\approx$340 Wh kg^{-1} in full-cell (all at 1 A g^{-1}).

2.3. Niobium Carbide /Nitride

Niobium carbide (NbC), being of high melting point (3610 °C), hardness, chemical stability, and wear resistance as well as good conductivity (4.6 mΩ cm^{-1} at room temperature and superconductivity at 12 K), shows a great prospect in the mechanochemical and microelectronic industries.[35] However, NbC usually needs to be acquired at high temperature, which limits its practical application. To date, three major preparation methods of NbC has been reported. 1) Directly mixing niobium source with carbon material under high temperature (>1000 °C). This approach enables NbC to bond tightly to carbon materials and maintain ideal morphology. For example, Xia and co-workers[36] used trichoderma spore carbon as growth matrix, on which Nb_2O_5 was loaded and then converted to NbC at high temperature (1200 °C) (**Figure** 5a–f). Resultantly, the reaction between Nb_2O_5 and carbon produced the spore carbon with advanced pore structures and increased specific surface area. Its mosaic structure with NbC embedding in carbon is beneficial to improve the electrical conductivity and cycling stability. 2) Reducing $NbCl_5$ and CCl_4 by active alkali metals ($M + NbCl_5 + CCl_4 \rightarrow MCl_x + NbC$, M is alkali metal, such as Na, Mg, etc.). The reaction temperature of this method is greatly decreased, but the reactive alkali metals and the confined space also limit its development and application (Figure 5g–i). By performing the magnesium thermal reaction (600 °C) in a high-pressure reaction kettle, Chen and co-workers[37] synthesized NbC as an intermediate material (NCM) to improve the performance of Li-S battery. The as-prepared NCM was proved to have a high conductivity and a strong ability to anchor soluble polysulfide (PS), effectively enhancing cyclic stability and rate capability. Conductive NCM intermediate layer acts as a shielding layer to restrict PS on the cathode side and prevent the passivation of lithium anode and self-discharge behavior of battery, also as a second collector to recycle the captured active material and significantly increase the sulfur utilization. 3) Max etching. This relatively mild preparation method can obtain NbC Mxene material with distinct lamellae structure. However, the synthesis of Max precursor also has limitations. Li and co-workers[38] prepared N-doped Nb_2CT_x (Figure 5j–l) with clear 2D lamellae structure for Li–S batteries. Specifically, 4.5 at% nitrogen can be doped into the Nb_2CT_x phase by reacting with urea. The doped N element expands the crystal cell volume of Nb_2CT_x and increases the ion transport path, conducing to the ion embedding. In fact, its c lattice parameters were expanded from 22.32 to 34.78 Å, and the corresponding reversible capacity was increased to 360 mAh g^{-1}. In addition, there are some special preparation approaches. For example, Liang and co-workers[39] acquired NbC with pulse laser. In a word, these aforementioned methods have some limitations and are not facile to scale up preparation (Figure 5).

Niobium nitride mainly include Nb_3N_5,[40] Nb_4N_3,[41] NbN[42] and some nonstoichiometric niobium compounds. Among them, the N-rich phase NbN_x can be divided into the following types:[43,44] 1) δ-NbN_x, $0.72 < x < 1.06$, belongs to NaCl-type lattice ($Fm\bar{3}m$ space group) with nitrogen atoms and vacancies arranged statistically, exhibiting high superconducting temperature (about 17.8 K). So, it is mostly used in cryoelectronic devices. 2) γ-Nb_4N_{3x} and γ-NbN_x, $0.72 < x < 0.84$, have body-centered cuboid structure ($I4/mmm$ space group). Herein, γ-NbN_x can be transformed into δ-NbNx above 1225 °C. 3) ϵ-NbN is assigned to the hexagonal crystal system of anti-WC lattice (CW, $P\bar{6}m2$ space group), being of the stable crystal system under 1330 °C. 4) δ'-NbN_x, $0.95 < x < 0.98$, is affiliated to the hexagonal system of anti-NIAS lattice (AsNi, P63/mmc space group), just appeared briefly during the transformation from δ-NbN_x to ϵ-NbN. Although the classification and crystal phase of niobium nitride have been reported, their conversion and transition mechanisms remain unclear.

Among niobium nitride, NbN with shrinking d-band and high state density near the Fermi level have good chemical stability with common electrolyte components and their decomposition products (such as HF), showing certain advantages in energy storage.[42] Notably, NbN has a good limiting effect on PS and can catalyze its conversion into LiS_2 Huo and co-workers[45] used NB@NG (mesoporous niobium nitride microspheres coated with N-doped graphene nanosheet) as the main multifunctional material of Li–S cathode, which achieves good capacity, efficiency and cycle life. First of all, its porous structure (as miniature reaction chamber to limit PS) and stable mechanical properties allow a large amount of reactive sulfur to be loaded. Second, polar NbN captures lithium polysulfide (LiPS) in cathode to prevent LiPS exudation by Nb–S chemical bonds, thus improving its circulation stability. Third, the strong electro-catalytic activity of NbN in accelerating LiPS redox reactions enhance the redox kinetics during cycling. Fourth, N-doped graphene provides high conductive network for NbN to enable electron transfer, thus achieving high power capability. Finally, graphene nanosheets wrapped on NbN microspheres mitigate LiPS' loss via physical limitations and N-hetero chemical anchorage (**Figure 6**a–h). In terms of these points, NB@NG shows large capacity (948 mAh g^{-1} at 1 C) and stability (only 0.09% reduction after 400 cycles) as lithium sulfur cathode material. Except electrode material, NbN also can be used as diaphragm coating by some studies (Figure 6).[46]

2.4. Niobium-Based Multielement Oxide

For the presence of two or more transition metals with multiple valence states and their possible synergies, the development of multiple transition metal oxides (TMOs) with multiple redox pairs has been verified to be an effective strategy to provide high specific capacity.[47] Different from the cell volume change by doping, the new phase structure generated by multiplex has direct gain effect on energy storage. Among niobium-based systems, the structure of multi-element oxide being well studied is M–Nb–O (M is the metal element).[48] Compared with unary Nb base materials, multi-materials can generally produce more

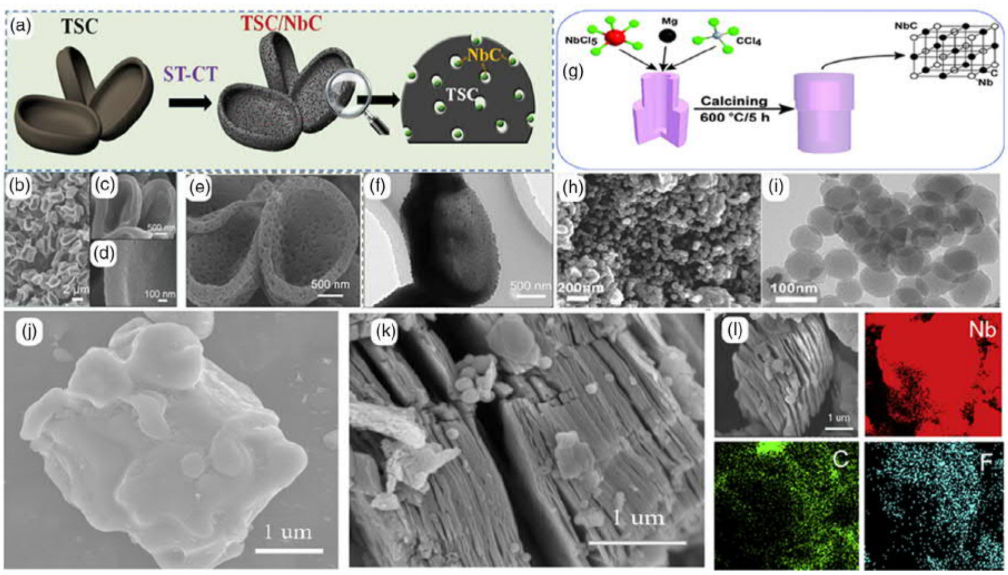

Figure 5. a–f) Synthetic procedure, SEM and TEM of NbC preparated by high temperature and g–i) low temperature; j–l) SEM of MAX, SEM and mapping of $NbCT_x$. a–f) Reproduced with permission.[36] Copyright 2019, Wiley-VCH. g–i) Reproduced with permission.[37] Copyright 2019 Wiley-VCH. j–l) Reproduced with permission.[38] Copyright 2019, Elsevier.

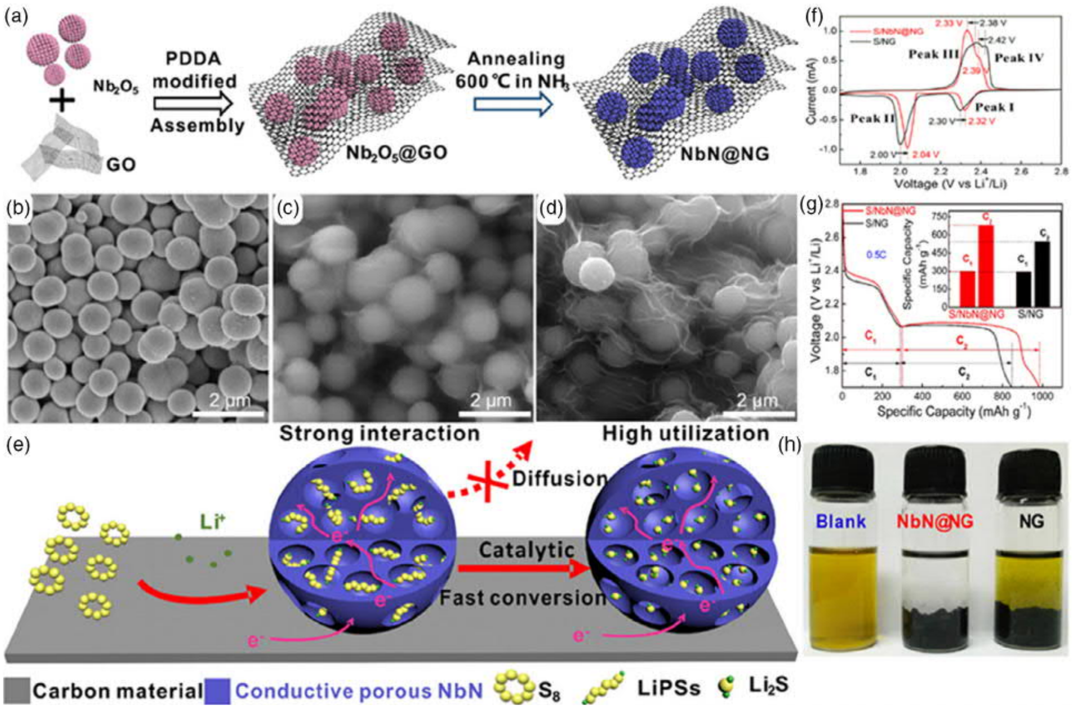

Figure 6. a) Synthetic procedure, b–d) SEM, e) schematic diagram of the LiPS adsorption and f) conversion processes, g) CV, typical voltage profile of S/NbN@NG and S/NG at 0.5C, and h) C_1 and C_2 represent the discharge capacities in stages 1 and 2, respectively (inset: corresponding discharge capacity in stages 1 and 2 for S/NbN@NG and S/NG) and LiPS adsorption performance. a–h) Reproduced with permission.[45] Copyright 2019, American Chemical Society.

redox reactions to improve specific capacity. For example, $TiNb_2O_7$ with Ti^{4+}/Ti^{3+} Nb^{5+}/Nb^{4-} and Nb^{4+}/Nb^{3+} redox pairs has theoretical capacity, higher than Nb_2O_5 (387.6 mAh g^{-1}).[49] It has been proved that multi-element oxide, being of better electrochemical and mechanical properties than unitary oxides and having synergistic effect among the multiple oxides, can elevate their performance in energy storage reaction. This work takes Ti–Nb–O system ($Ti_2Nb_{2x}O_{4+5x}$) as an example to introduce niobium base multi-element oxide.

Apart from the aforementioned advantages, the working potential of $Ti_2Nb_{2x}O_{4+5x}$ within 1.0 and 2.0 V, higher than the decomposition potential of common electrolyte (<0.8 V) and dendrite growth potential (<0.2 V), shows good security.[50] For another, $Ti_2Nb_{2x}O_{4+5x}$ has shear ReO_3-type crystal structure, which consists of a few tetrahedrons (0–4%) and octahedrons with shared angles and/or edges—greatly stabilizing the crystal structure during the energy storage process. Since 1950, the Ti–Nb–O system has been studied.[51] Specifically, $TiNb_2O_7$, first explored at 2011, has attracted extensive attention due to its unique zero-strain performance similar to $Li_4Ti_5O_{12}$. Moreover, despite a high lithium potential (1.64 V, close to $Li_4Ti_5O_{12}$), $TiNb_2O_7$ has a large theoretical capacity of 387.6 mAh g^{-1} due to its five-electron transfer reaction.[52] Goodenough and co-workers[53] studied the change rule of phase structure and element valence of $TiNb_2O_7$ in energy storage by in situ XRD and X-ray absorption near-edge spectra (XANES). Here, the structural changes can be divided into three phases: two solid solution states and two-phase coexistence state. The former can be composed of $Li_0TiNb_2O_7$ and $Li_{1.75}TiNb_2O_7$ conversion into $Li_1TiNb_2O_7$ and $Li_{3.6}TiNb_2O_7$, respectively, whereas the latter is in between them. Due to Li^+ insertion and accumulation, clear expansion appeared on (010) lattice plane, and the $TiNb_2O_7$ cell volume of before and after Li^- embedding ($TiNb_2O_7$ and $Li_{3.6}Nb_2O_7$) increased by 7.22%. But it still achieves good cycling performance by reason of the cushioning effect of porous structure (retains 84% capacity after 1000 cycles). According to XANES test, the reduction of Ti^{4+} and Nb^{5+} ions start at the same speed during lithiation process. When fully discharged to 1.0 V, the oxidation states of Ti and Nb are approximately +3.2 and +3.6, consistent well with the XRD result (discharge capacity is ≈281 mAh g^{-1}). In particular, no clear side reaction also verifies its high reversibility (**Figure 7**).

Again for $Ti_2Nb_{2x}O_{4+5x}$ system, more substance has been studied or just begun to be studied. Shu and co-workers[54] proposed a new approach to coat $TiNb_{24}O_{62}$ with N-doped carbon layer, and further investigated its Li^+ storage mechanism and crystal phase changes. The organic gas from ethylenediaminetetraacetic acid (EDTA) pyrolysis were repyrolyzed on the surface

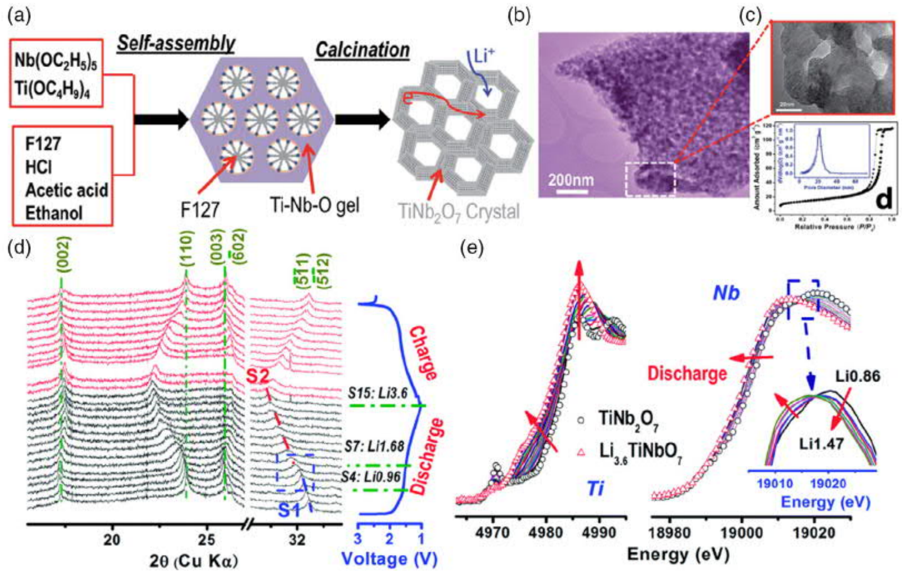

Figure 7. a) Schematic diagram of the formation mechanism for nanoporous $TiNb_2O_7$. b) TEM image of TNO-700. c) HR-TEM image of TNO-700. d) Nitrogen adsorption-desorption isotherm and corresponding pore size distribution curve (inset) for TNO-700. In situ XRD patterns collected during initial discharge and charge at a constant current rate of C/8 between 1.0 V and 3.0 V. e) In situ Ti K-edge and Nb K-edge XANES spectra collected during initial discharge at C/10 rate between 1.0 V and 3.0 V voltage range (inset figure: the isosbestic point on the spectra between x=0.86 and x=1.47 indicates a two-phase reaction region). a–e) Reproduced with permission.[53] Copyright 2014, Royal Society of Chemistry.

of $TiNb_{24}O_{62}$ particles fiber, to form N-doped carbon layer with the controllable homogeneous thickness of 2 nm. Also, a large number of defect sites derived from N-doped carbon layer effectively improve the conductivity and electrochemical activity; the small particle structure can shorten the ion transport path; $TiNb_{24}O_{62}$ has stable structure and high Li^+ diffusion channel. The aforementioned effective combination ensures its excellent electrical energy storage properties (218 mAh g^{-1} at 0.5 C) (**Figure 8**).

$Ti_2Nb_{2x}O_{4+5x}$, as the most studied Nb-based multi-element oxide, gradually established its research system. In addition, a variety of new phases, niobium-based multicomponent oxides are summarized and listed in **Table 1**. Their new phase are synthesized by combining Nb with different metals, showing good electrochemical performance. More precisely, niobium-based multi-element oxide generally have higher capacitance than niobium oxide because of the increase in redox electron pairs. However, these new phases are limited to be studied within the small-sized Li^+ systems and low-energy-density SCs, whereas the research of sodium systems or other polyvalent metal ion systems remains to be done.

2.5. Other

Except for the aforementioned Nb-based materials, there are also a few reports on $NbSb_2$. Varadaraju and Reddy[55] applied $NbSb_2$ in LiB and analyzed its energy storage mechanism. Here, $NbSb_2$ has $OsGe_2$-type crystal structure, namely two $NbSb_8$ tri-prism (Nb surrounded by 8 Sb) forms a double-capped tri-prism structure of Nb—Nb covalent bond through shared rectangular surface. According to $NbSb_2+6Li^++6e^- \leftrightarrow 2Li_3Sb + Nb$, the theoretical capacitance can be up to 480 mAh g^{-1}. Multi-cycle CV tests were conducted in the range of 0–2 V, and its first cycle mechanism was proposed by combining XRD and peak potential

Discharge process

$$NbSb_2 + 5.4Li \rightarrow 1.8Li_3Sb + 0.9Nb + 0.1NbSb_2$$

Charge process

$$1.8Li_3Sb \rightarrow 1.4Sb + 4.2Li + 0.4Li_3Sb$$

From this mechanism, the poor cyclic stability of $NbSb_2$ can be inferred (the cyclic stability test also supports this point). The suppression of adverse phase transition is one of the research directions to optimize $NbSb_2$ performance (**Figure 9**).

Moreover, Nb is often used as doped atoms to modify and optimize other materials as well as the main energy storage material. For example, Zhou and co-workers[56] doped Nb into lithium manganese based anode material to improve its electrochemical performance. Herein, compared with Mn, the higher binding energy of Nb–O and larger Nb ion size can well inhibit O separation during lithium inset and expand ion transport channels. After doping Nb, the potential interval between redox peaks of Li–Mn base anode material diminished, evidencing its increased electrochemical reversibility and reduced polarization. By the impedance test, the Nb-doped material enhances the impedance

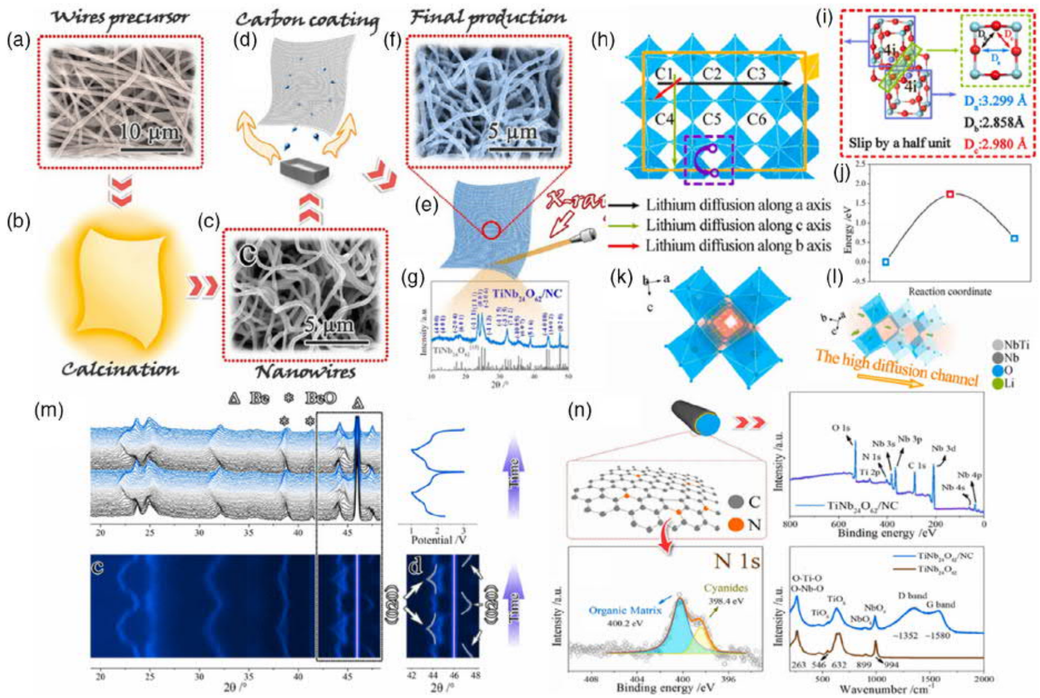

Figure 8. a–g) Schematic illustration of the fabrication strategy for $TiNb_{24}O_{62}$/NC nanowires. h) Diffusion paths for lithium ion within the cubic–like cavities along different directions; i) Local environment at the edge of two adjacent rectangle building blocks and j) The corresponding lithium ion diffusion barrier; k, l) Schematic illustrations of the high diffusion channel for lithium ion. m) In–situ XRD patterns of $TiNb_{24}O_{62}$/NC nanowires during cycling. n) XPS of $TiNb_{24}O_{62}$/NC nanowires. a–n) Reproduced with permission.[54] Copyright 2016, Elsevier.

(118.2 Ω, lower than the initial 254.5 Ω) and ion transfer rate (1.16×10^{-18}, better than the original 8.88×10^{-19}). According to density functional theory (DFT) calculation, strong Nb—O bond and small Li^+ migration barrier can effectively stabilize material structure and accelerate Li^+ diffusion after Nb doping. Furthermore, oxygen vacancy formation in Nb-doped structure requires high energy, making its quantity reduced. In conclusion, appropriate Nb-doping effectively stabilized material structure, inhibited vacancy increase, accelerated Li^+ diffusion, and increased the electrochemical properties of material.

In conclusion, Nb-based materials for energy storage systems are abundant, but their many energy storage mechanisms and phase transitions still need to be further investigated. To date, the common characteristics of different energy storage systems from Nb-based materials have been summarized, as shown in the following table (**Table 2**).

3. Application of Nb-Based Materials

3.1. Lithium-Ion Battery

As the main storage device for portable electronic products and power systems, LIB has the advantages of high energy density, long cycle life, and good environmental compatibility, which plays a crucial role in our daily life.[57] A typical LIB device is composed of anode (as graphite) and cathode (as $LiCoO_2$). During charging, Li^+ are pumped out of the cathode body, pass through the electrolyte, then inserted into the anode. The discharge process is reversed.[58] Although such batteries are commercially successful, they still have some drawbacks, such as insufficient safety and capacity. Developing new high-efficiency electrode materials is one of the key strategies to relieve these problems.[59] Notably, Nb-based materials have aroused great interest due to their high security and capacitance advantages. In LIB, their redox potentials (1.0–2.0 V) matched with the lowest unoccupied molecular orbital (LUMO) of organic liquid carbonate electrolyte, thus avoiding the formation of passivated solid electrolyte interface (SEI) layer.[8] Compared with the traditional $Li_4Ti_5O_{12}$ (140 mAh g^{-1}), Nb-based materials generally has a higher capacitance due to its polyvalent properties.

To date, there are many reports on the application of Nb-based materials, most of which are used as LIB electrode materials. Here, stable morphological structure and appropriate ion transport path are one of the design directions of LIB electrode materials. For example, Shu and co-workers[60] prepared $K_2Nb_8O_{21}$ microtubules (outer diameter 2 μm, wall thickness 500 nm) and $K_2Nb_8O_{21}$ nanotube (outer diameter 160 nm, wall thickness 40 nm) by controlling the voltage and speed of electrostatic

Table 1. Niobium based multi-element oxide for energy storage.

Material	Fabrication method	Research areas	Specific capacity	Reference
$AgNb_{13}O_{33}$	Solid-state reaction	LIB	329.4 mAh g^{-1} at 0.1 A g^{-1}	[166]
$ZrNb_{14}O_{37}$	Electrospinning	LIB	244.9 mAh g^{-1} at 0.1 A g^{-1}	[114]
$Bi_5Nb_3O_{15}$	Electrospinning	LIB	372 mAh g^{-1} at 0.1 A g^{-1}	[167]
BNb_3O_9	Electrospinning	LIB	126.8 mAh g^{-1} at 0.9 A g^{-1}	[116]
$FeNb_{11}O_{29}$	Electrospinning	LIB	272.6 mAh g^{-1} at 0.1 C	[168]
$TiNb_2O_7$	Hard templates	LIB	387 mAh g^{-1} at 1 C	[169]
$TiNb_6O_{17}$	Electrostatic spraying	LIB	214.4 mAh g^{-1} at 0.5 C	[170]
$Ti_2Nb_{10}O_{29}$	Solid composite	LIB	258 mAh g^{-1} at 0.03 A g^{-1}	[171]
$MnNb_2O_6$	Hydrothermal	SC	400 F g^{-1} at 0.5 A g^{-1}	[172]
$CrNb_{49}O_{124}$	Electrospinning	LIB	340 mAh g^{-1} at 0.06 A g^{-1}	[173]
$MoNb_{12}O_{33}$	Solvothermal	LIB	321 mAh g^{-1} at 0.1 C	[174]
$BaNb_{3.6}O_{10}$	Electrospinning	LIB	263.8 mAh g^{-1} at 0.1 A g^{-1}	[143]
$CrNb_{11}O_{29}$	Hydrothermal	LIB	343 mAh g^{-1} at 0.1 C	[113]
$GeNb_{18}O_{47}$	Electrospinning	LIB	216.9 mAh g^{-1} at 0.1 A g^{-1}	[175]
$Mg_2Nb_{34}O_{87}$	Solvothermal	LIB	338 mAh g^{-1} at 0.1 C	[176]
$ZrNb_{24}O_{62}$	Electrospinning	LIB	320 mAh g^{-1} at 0.1 C	[177]
KNb_3O_8	Solid-state reaction	SIB	166 mAh g^{-1} at 0.003 A g^{-1}	[178]
$Sn_2Nb_2O_7$	high temperature calcination	SIB	300 mAh g^{-1} at 0.1 A g^{-1}	[139]
$AlNbO_4$	Solid-state reaction	LIB	291 mAh g^{-1} at 0.014 A g^{-1}	[179]
$Nb_{18}W_8O_{69}$	Solid-state reaction	LIB	265 mAh g^{-1} at 0.5 C	[180]

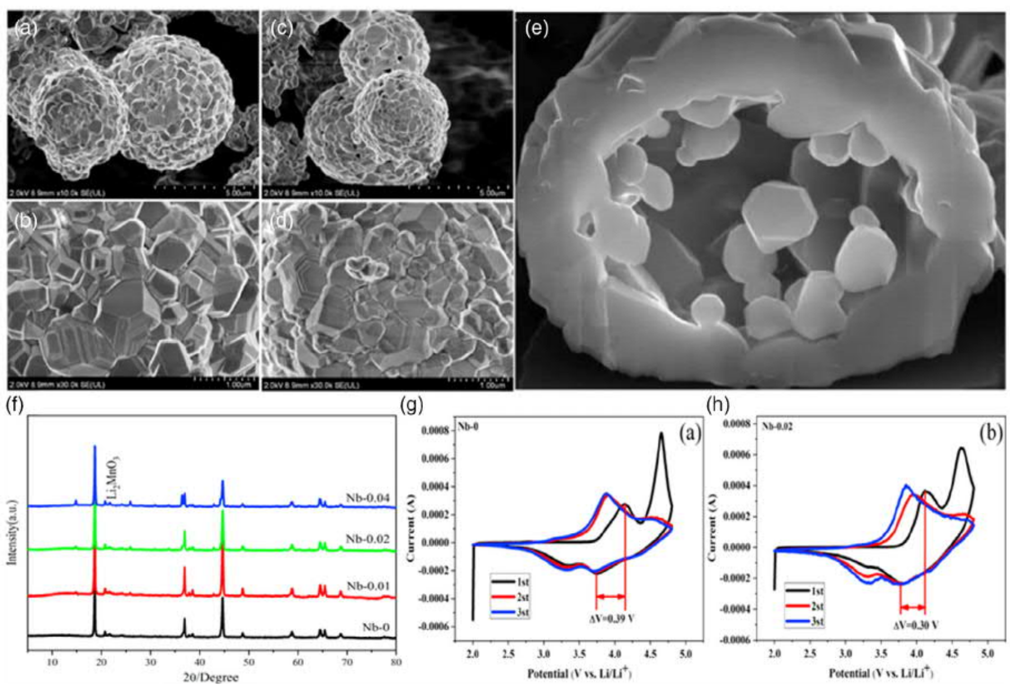

Figure 9. a–e) SEM images of pristine and Nb-doped $Li_{1.2}Ni_{0.13}Co_{0.13}Mn_{0.54}O_2$. f) Powder XRD patterns of Nb-0, Nb-0.01, Nb-0.02, and Nb-0.04, CV analysis of g) Nb-0 and h) Nb-0.02. a–h) Reproduced with permission.[56] Copyright 2020, Elsevier.

Table 2. Niobium based materials for energy storage.

Materials	Advantages	Disadvantages	Areas
NbO	Good electrical conductivity, low strain, safe working potential	Poor thermal stability	LIB
NbO_2	High capacitance, safe working potential	Poor electrical conductivity	LIB
$Nb_{12}O_{29}$	Safe working potential, good electrical conductivity, developed crystal structure	Limited theoretical capacity	LIB, SIB
T-Nb_2O_5	Large lattice channels, low strain response, safe working potential, without diffusion limitation of solids	Limited theoretical capacity, poor electrical conductivity	LIB, SIB, SC, Li–S, KIB
H-Nb_2O_5	Fast ion-transport path, safe working potential	Transmission anisotropy, asynchronous phase change	LIB
NbS_2 /$NbSe_2$	2D lamellar structure, safe working potential	Too much irreversible loss, large volume effect	LIB, SIB
NbC	High stability, safe working potential, good electrical conductivity	Difficult to preparation	Li-S, SC
NbN	High stability, limiting effect on polysulfide, safe working potential, polarity, electrocatalytic activity	Difficult to preparation	Li-S
$Ti_2Nb_{2x}O_{4+5x}$	High theoretical capacity, low strain response, safe working potential	Poor electrical conductivity	LIB, SIB, SC
Others	–	–	–

spinning. Its crystal structure is orthogonal tungsten bronze composed of NbO_6 octahedron. Locally, most Nb is located in the center of eight planes, and the remaining Nb and K fill the pentagram tunnel. The peaks at ≈1.61 and ≈0.70 V correspond to the redox reactions of Nb^{5+}/Nb^{4+} and Nb^{4+}/Nb^{3+}, respectively. According to in situ XRD and transmission electron microscopy (TEM), $K_2Nb_8O_{21}$ shows high structural stability (80.3% capacity is maintained after 5000 cycles) and electrochemical reversibility (the lattice changes periodically) as anode material for LIC. The Li^+ diffusion coefficients can be determined from CV results using the Randles–Sevcik equation. More precisely, Ip is proportional to the square root of the sweep rate $\nu^{0.5}$, so the Li^+ diffusion coefficient (D_{Li+}) can be calculated based on the Randles–Sevcik equation

$$Ip = 2.69 \times 10^5 \times n^{1.5} \times SCD^{0.5}\nu^{0.5} \tag{6}$$

where S, C, and n are the surface area of electrode, Li^+ concentration, and the number of electrons transferred in reaction, respectively. According to this equation, nanotubes have better electrochemical performance due to their high specific surface area and short ion transport path. Apart from being electrode material, the Nb modification for solid electrolyte has also been reported. For example, Markovic and co-workers[61] doped Nb in garnet $Li_7La_3Zr_2O_{12}$, not as the energy storage main material, to stabilize the diffusion interface of Li^+. This review does not give it too much explanation (**Figure 10**).

Diversified Nb-based materials show excellent and different electrochemical properties in LIC, while the main redox electron pairs (Nb^{5+}/ Nb^{4+} and Nb^{4+}/ Nb^{3+}) generated by Nb in energy storage process are similar. Furthermore, they are mostly embedded materials with good stability and safe working potential in LIB. Their main difference lies in the stability and ion reachability arised from distinct morphologies, the change of ion transport path caused by crystallinity and lattice parameters, and the synergistic effect of distinct metals/nonmetals.

3.2. Sodium Ion Battery

SIB, with basic storage mechanism similar to LIB, is considered as a promising large-scale energy storage device because of its low cost and abundant Na reserves.[62] However, its development is far behind due to low energy density and slow Na^+ diffusion kinetics by reason of the larger ion size of Na^+ ($R_{Na^+} = 1.02$ Å $> R_{Li^+} = 0.76$ Å).[2] Accordingly, Nb-based materials with lattice channels and low energy storage strain have the potential to be used in SIB. Under the premise of intrinsic advantages, further improving materials stability and active sites quantity and utilization is the focus of research. The 1D nanofiber (T-Nb_2O_5@C) encapsulated with ultra-small T-Nb_2O_5 crystal obtained by Zhou and co-workers[22] has good electrochemical performance. Carbon matrix can enhance the electrical conductivity, inhibit T-Nb_2O_5 nanoparticles aggregation and materials crushing, and improve the cyclic stability (the same capacity within 5000 cycles). The uniformly distributed ultrafine nanoparticles (6–8 nm) give full play to Nb_2O_5 capacitive characteristics and improve material capacitance (229 mAh g^{-1} at 0.1 A g^{-1}). Aside from carbon and nanocrystallization, the lattice design is also an effective approach to optimize the performance of Nb-based materials. High-crystallinity nanomaterials and amorphous membrane materials display surprisingly high capability in SIB. Yu and co-workers[63] introduced an amorphous hydrogenated Nb_2O_5 film with self-sequencing porous structure (15–20 nm) growing on Nb substrate. This design with the ordered porous structure enables the Nb_2O_5 film to directly contact with the substrate, promoting efficient ion transport. Moreover, this structure ensures the elastic adhesion of nanoporous film to the flexible substrate, avoiding the loss of structural integrity due to multiple Na^+ embedded/disembedded. Finally, hydrogenation gives the insulator Nb_2O_5 higher electronic conductivity (3.0×10^{-3} S cm^{-1}, larger than nonhydrogenation). Its large capacitance (185 mAh g^{-1} at 0.5 C) and excellent cycling stability demonstrate that the Na^- storage activity and durability of electrode materials can be effectively promoted by structural optimization (amorphous), composition regulation

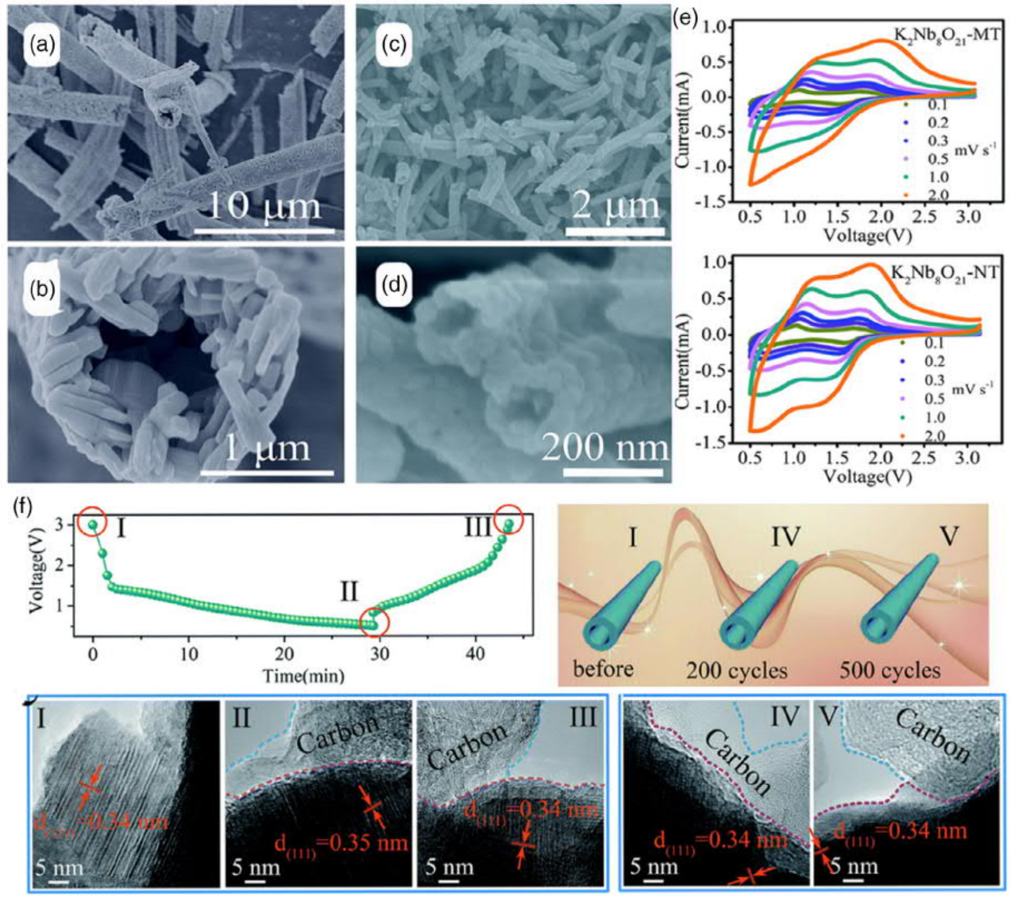

Figure 10. a,b) SEM of $K_2Nb_8O_{21}$-MT and c,d) $K_2Nb_8O_{21}$-NT and e) CV of them. f) Ex situ HRTEM images of $K_2Nb_8O_{21}$-NT at different lithiated/delithiated states: Pristine (I) discharge to 0.5 V(II) and recharge to 3.0 V(III). After 200 cycles (IV) and 500 cycles (V). a–f) Reproduced with permission.[60] Copyright 2018, Royal Society of Chemistry.

(hydrogenation), and morphology design (ordered nanopore) (**Figure 11**).

Compared with LIB, few studies about Nb focused in SIB. The mechanism of energy storage and interfacial ion exchange need to be further studied.

3.3. Potassium-Ion Battery

Potassium-ion battery (KIBs), being of the low redox potential (−2.94 V vs standard hydrogen electrode) of potassium with natural abundance, results in high energy density at the operating voltage.[64] The large ion size (1.38 Å, larger than Na^+) leads to slow K^+ diffusion rate and serious volume expansion for most of electrode materials during K^+ embedding/disembedding process.[65] Resultantly, the development of KIBs has been limited and the study is still in its infancy. So far, very little material has shown promising results in KIBs.[66]

In theory, T-Nb_2O_5 with very large (001) lattice spacing, can satisfy the requirements of K^+ diffusion and embedding.[67] In addition, its fast pseudo-capacitive response ensures excellent rate capability, which has been demonstrated in Li/Na batteries.[68–70] Therefore, it has the potential to be applied in KIBs. Tang and co-workers[70] first report hierarchical urchin-like Nb_2O_5 nanomaterial assembled by nanowires as KIB anode, and detailed intercalation–pseudocapacitive behavior of the T-Nb_2O_5 material was also explored. Specifically, the XRD of T-Nb_2O_5 did not change after many cycles, which verified the fact of large lattice channel. Second, the constant current intermittent titration test also proved its high K^+ diffusion coefficient (3×10^{-10} $cm^2\ s^{-1}$), which unexpectedly reached the same order of magnitude as Li^+. Of course, except from the lattice advantage of T-Nb_2O_5, this phenomenon may also be related to K^- weak solvation. This report assembled both potassium half-cell and potassium dual-ion battery (KDIB), with T-Nb_2O_5

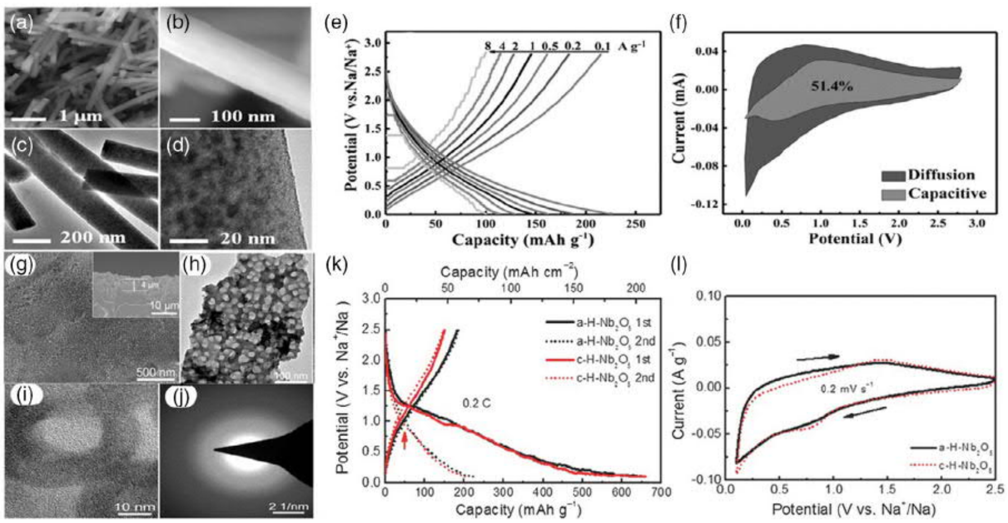

Figure 11. a,b) SEM, c,d) TEM, e) GCD and f) CV of T-Nb_2O_5@C.[22] g,h) SEM, i,j) TEM, k) GCD, and l) CV of T-Nb_2O_5 membrane.[63] a–f) Reproduced with permission.[22] Copyright 2017, Wiley-VCH. g–l) Reproduced with permission.[63] Copyright 2017, Wiley-VCH.

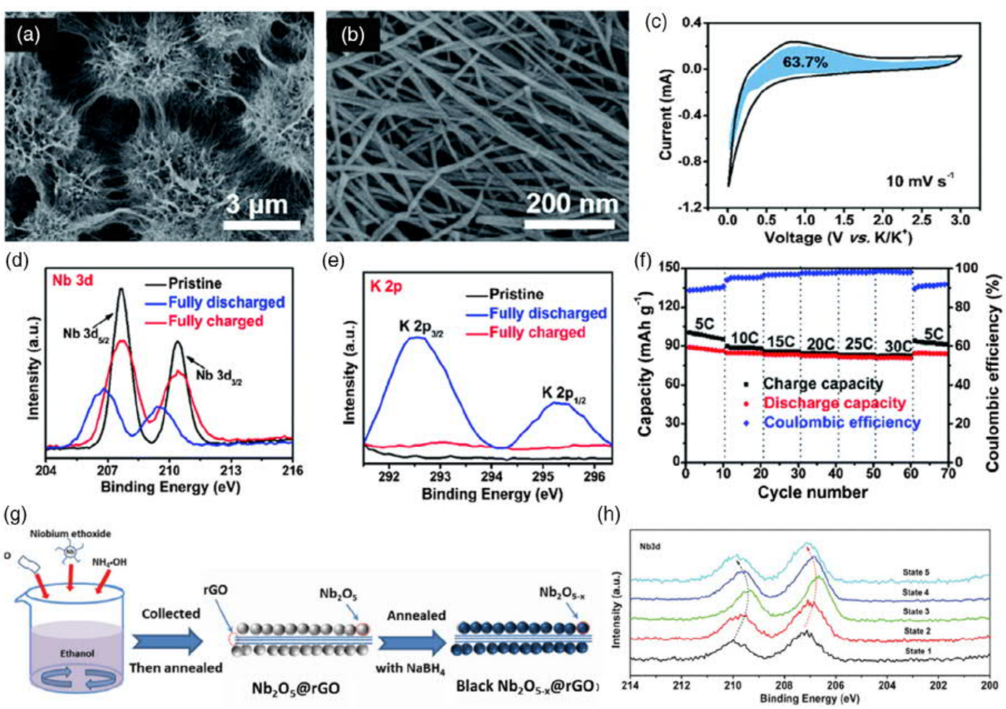

Figure 12. a,b) SEM, c) CV, d,e) XPS and f) rate capability of T-Nb_2O_5;[70] g) Synthesis procedure and h) ex situ XPS test of the black Nb_2O_{5-x}@rGO nanosheets.[68] a–f) Reproduced with permission.[70] Copyright 2018, Royal Society of Chemistry. g–h) Reproduced with permission.[68] Copyright 2019, Wiley-VCH.

as cathode, graphite as anode, and 0.8 M KPF_6 in EC:PC:DMC: EMC = 2:2:3:3 (volume ratio) as electrolyte. During charging, K^+ ions were embedded into T-Nb_2O_5 to form $K_xNb_2O_5$. At the same time, PF_6^- anions are inserted into the graphite to produce C_xPF_6. The charging process is opposite. All in all, it has excellent rate capability and cyclic stability due to its fast electrochemical kinetics and suitable K^+ rapid diffusion channel (**Figure 12**).

The Nb-based materials and their polyphase composite, and interface optimization are effective ways to improve the performance in KIBs. Lee[68] used Nb-based materials embedded with graphite, optimized by surface engineering design (noncrystallizing and vacancy defect), to assemble the whole battery, showing good electrochemical performance (negligible capacity degradation after 3500 cycles at 1500 mA g^{-1}). Its main electrochemical advantage lies in: 1) Embedded graphene and defect structure improve the poor electrical conductivity. 2) Defects and amorphous surface layers promote surface capacitor storage. 3) Good electroactive mesoporous afforded the effective contact between material and electrolyte. In general, Nb-based materials have good energy storage potential in KIBs, mainly due to their small energy storage volumetric strain and large ion transport channel. However, limited by the insufficient research and development of KIBs, the application of Nb-based materials is also less, and its energy storage mechanism and optimization mode remain to be studied in future.

3.4. Lithium–Sulfur Battery

Li–S with its high theoretical energy density (2500 Wh kg^{-1}) is regarded as one of the most competitive candidates to surpass the LIC.[71,72] However, several problems must be overcome before actual application, such as shutting down behavior as a result of high PS solubility, sulfur insulation and its lithiated products, and slow transformation kinetics of the intermediate LiPS.[73] Due to strong sulfur constraint of micropores and enhancement of electron conductivity, porous carbon has been deemed as beneficial host material for Li–S.[74] However, the poor LPS affinity of nonpolar carbon materials limits their immobilization and reduces sulfur dynamics, resulting in unsatisfactory shuttle inhibition and low coulomb efficiency.[75] Polar Nb-based materials as sulfur accelerators, with strong LPS affinity and good chemical stability, have significant advantages to improve Li–S electrochemistry performance. The regulation of the crystallinity and defect structure has been acted as an effective method to promote electron/ion transfer and sulfur fixation/catalysis of Nb-based materials in Li–S. Vacancy in niobium-based materials further enhanced the chemical bonding with LPS and reduced the activation energy of sulfur redox reaction. Chen and co-workers[76] implanted ultrafine Nb_2O_{5-x} nanocluster with amorphous structure and rich oxygen-vacancy into the micropores of carbon nanosphere to form strawberry-like nanostructure, improving the performance of Li–S. Also, amorphous and defective structures elevated the affinity of Nb_2O_5 to LPS, and oxygen vacancy further increased the catalytic activity of LPS conversion. Furthermore, nanocluster embedded composite structure can be used as nano-reactor to limit sulfur uniform distribution, improve sulfur utilization, provide conductive framework to accelerate electron/ion transfer and rich active interface for LPS restriction and conversion, thereby improving electrochemical performance (**Figure 13**).

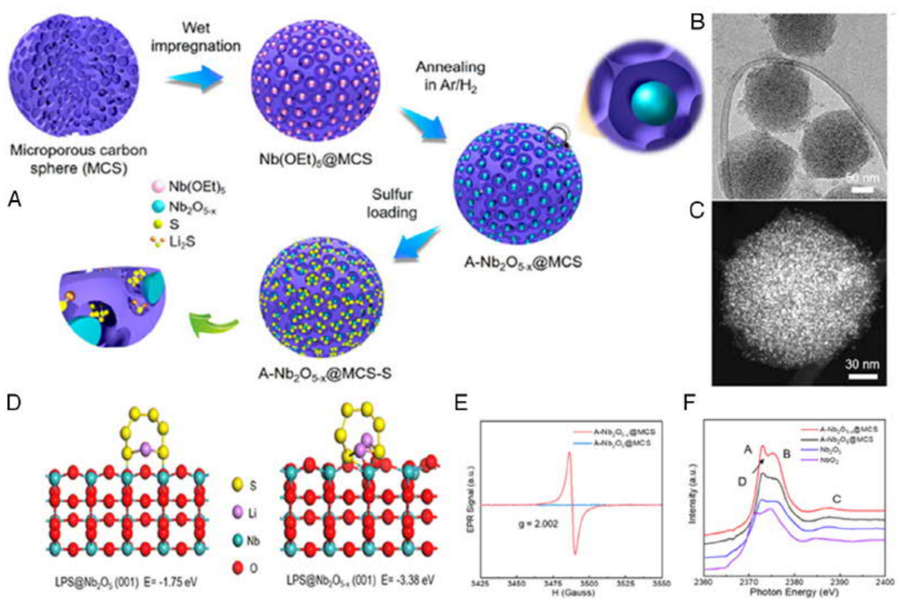

Figure 13. A) Synthetic process, B,C) TEM and STEM of A-Nb_2O_{5-x}@MCS. D) Optimized geometric configuration and corresponding $Li_2S_6E_{ads}$ of T-Nb_2O_5 (001) and Nb_2O_{5-x} (001). E) EPR pattern and (F) Nb L_3-edge XANES spectra of A-Nb_2O_{5-x}@MCS.[76] A–F) Reproduced with permission.[76] Copyright 2020, American Chemical Society.

ADVANCED ENERGY & SUSTAINABILITY RESEARCH
www.advenergysustres.com

Thanks to the polarity and affinity of niobium-based materials to LPS, the preparation of materials with cavity structure has a good application prospect in Li–S batteries. Wang and co-workers[77] integrated hollow Nb_2O_5 microspheres (2–3 μm) with highly conductive graphene oxide to construct hybrid shell material with excellent ionic/electronic conductivity (M-Nb_2O_5@rGO). Polar Nb_2O_5 has fast Li^+ transmission channel and stable chemical interaction with PS, promoting PS transformation into Li_2S. The huge pore space with high sulfur load significantly alleviates the sulfur volume expansion during energy storage process. Meanwhile, rGO surrounding the electrode will further enhance the redox kinetics of Nb_2O_5. Due to this design advantage, M-Nb_2O_5@rGO, as the Li–S main electrode material, can obtain 1004.5 mAh g^{-1} capacitance at the current density of 0.2 C (**Figure 14**).

In Li–S, the polar Nb-based materials are expected to substitute the carbon as the highly stable materials, which can effectively limit LPS. By means of its advantages, the porous cavity and vacancy defects are designed to further improve its performance in Li–S. However, compared with the Li–S theoretical capacity, there is still a large space for its future improvement.

3.5. Supercapacitors

SC with high power density and extended life is an excellent candidate for efficient energy conversion device, but the low energy density limits its development and application.[6] Herein, building hybrid SC, composed of metallide cathode and activated carbon anode, is an effective strategy to increase the energy density.[78] Hybrid capacitors, accumulated charge from the Faraday redox reaction, can achieve high specific capacitance and operating voltage window, resulting in large energy density.[79] However, this kind of energy storage device has high requirements for cathode materials, such as fast ion embedding rate.[80] Interestingly, Nb-based materials with suitable ion diffusion channels can meet the requirements. Moreover, its safe working potential and desirable specific capacity are also its applicable advantages. For example, Shen and Wang[81] successfully manufactured hybrid capacitor with high energy density (110.4 Wh kg^{-1}) and power density (5464 W kg^{-1}) using $TiNb_2O_7$@carbon fiber (TNO@C) as anode and carbon fiber (CFs) as cathode. TNO@C, the 1D fiber material prepared by electrostatic spinning, composed of TNO particles and intergranular carbon layer to enhance TNO conductivity. To be specific, TNO@C, with capacitive behavior controlled by Faraday redox reaction, showed excellent electrochemical performance (remains above 77% after 1500 cycles) in lithium semi-batteries and hybrid capacitors due to its 2D lattice gap space, as well as the enlarged conductivity and toughness of carbon coatings (**Figure 15**).

Most of the aforementioned hybrid capacitors use organic electrolytes, being of high cost and harsh operating environment with difficulty in application.[82] In contrast, aqueous electrolyte are popular because of their advantages such as high safety, low

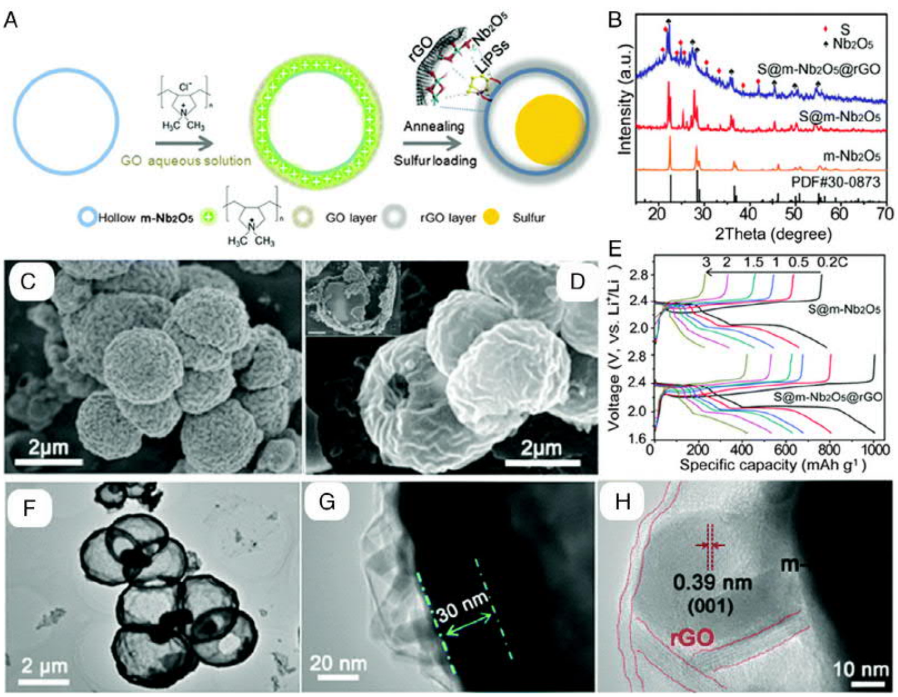

Figure 14. A) Synthetic process, B) XRD, C–D) SEM, E) GCD, F–H) HRTEM of Nb_2O_5@rGO.[77] A–H) Reproduced with permission.[77] Copyright 2019, Royal Society of Chemistry.

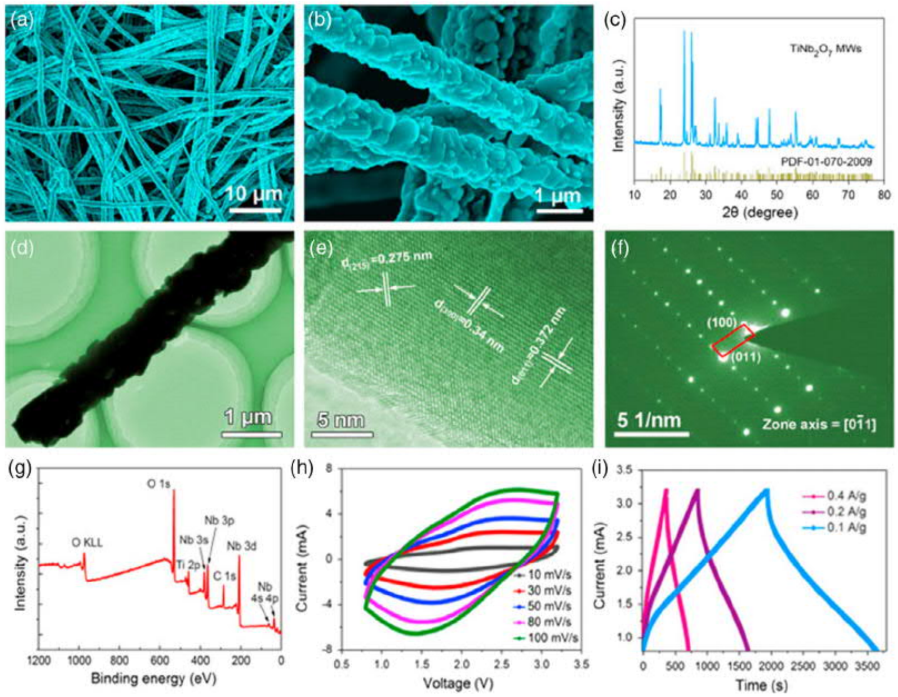

Figure 15. a,b) SEM images and c) XRD pattern of the TNO MWs. d) TEM image of a single TNO MW. e) HRTEM and f) SAED pattern of the TNO nanocrystalline. g) XPS of TNO@C MWs, h) CV and i) GCD of TNO@C//CFs hybrid Li-SC.[81] a–i) Reproduced with permission.[81] Copyright 2015, Elsevier.

cost, and simple operation conditions.[83] The Nb-based materials also showed good electrochemical performance in aqueous SC. Zhang et al.[84] successfully prepared N-doped graphene (NG) using 5-hydroxymethylfurfural (5-HMF) as carbon source and urea as nitrogen source through a simple pyrolysis route. Subsequently, Nb_2O_5 nanosheets were homogeneously grown on N-doped graphene to produce T-Nb_2O_5/3DNG as SC cathode material. Also in this work, $NiCo_2S_4$ growing on nickel foam is used for SC anode material. As for the assembled resultant SC devices in three-electrode system (−1 to 0.2 V, KOH aqueous solution), a wide redox peak (about −0.6 V) of T-Nb_2O_5/3DNG was observed due to the pseudocapacitor behavior, which was induced by N-heterotom and the Faraday reaction ($Nb_2O_5 + OH^- \Leftrightarrow Nb_2O_5OH + e^-$) on T-$Nb_2O_5$ surface. Meanwhile, via their synergistic effect, T-Nb_2O_5/3DNG delivered high specific capacitance (952.7 F g^{-1} at 1 A g^{-1}). Fixed action and buffer space from 3DNG optimize T-Nb_2O_5 cyclic stability (over 90.8% after 5000). Resultantly, this SC afforded high energy density and power density (81.37 Wh kg^{-1} and 9568.3 W kg^{-1}) (**Figure 16**).

Still for hybrid capacitor, Nb-based materials with large ion transfer channels is well adapted to the fast double-layer nature of counter electrode, showing high cyclic stability and energy density, but its capacity needs to be further improved. With regard to the aqueous system, Nb-based materials have good pseudocapacitive energy storage reaction to provide high specific capacitance, while the limited potential window and polarization phenomena still limit their further development.

3.6. Others

Rechargeable aluminum ion batteries (RAIB) based on trivalent aluminum (Al) have several unique advantages over other multivalent ion batteries.[85] First of all, Al is the most abundant metal element in the Earth's crust. Meanwhile, mature aluminum mining can greatly reduce RAIB costs.[86] Second, the trielectron redox reaction of Al^{3+}/Al produces very high theoretical specific capacity (2980 Ah kg^{-1}) and volume capacity (8046 Ah L^{-1}).[87] In addition, the low flammability and toxicity with high stability of Al metal electrodes make RAIB relatively safe. Therefore, it has aroused extensive attention and research interest in academia. Also by virtue of the large ion transport channel and low strain, Jin and co-workers[88] prepared single-crystal Nb_2O_5 nanotubes by chemical vapor deposition (CVD) method, and systematically studied their electrochemical properties as RAIBs electrode materials. The obtained Nb_2O_5 with thin wall, hollow structure, and high porosity provides a short diffusion distance for charge carrier transmission, thus achieve excellent ion insertion/extraction rate. Embedded mechanism of $AlCl_4^-$ can be observed clearly by the mappings of different charge and

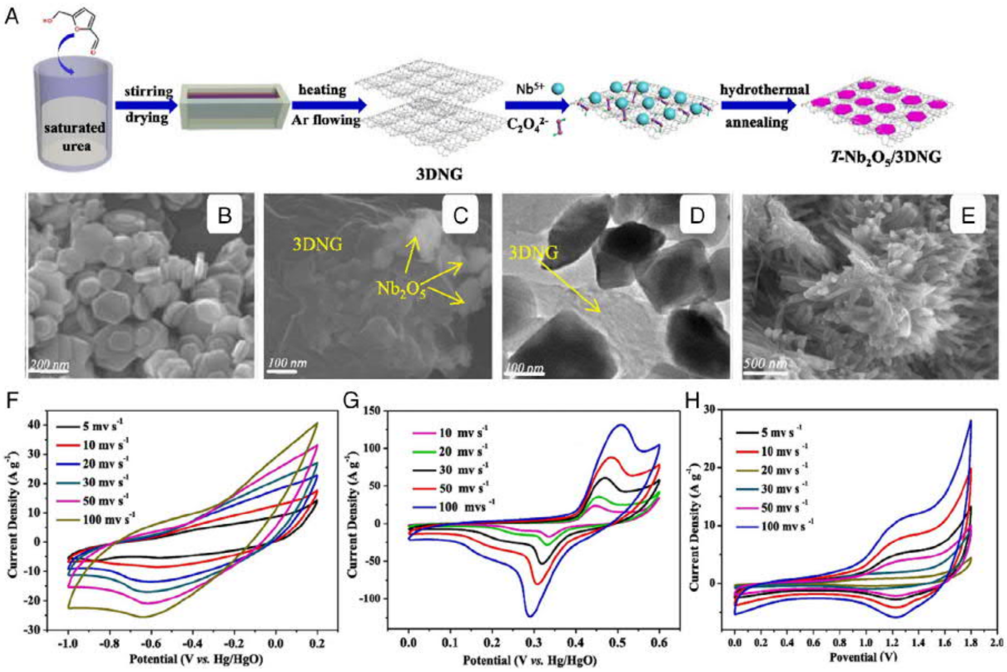

Figure 16. A) Synthetic process, B,C) SEM and D) TEM of T-Nb_2O_5/3DNG. E) SEM of $NiCo_2S_4$. F) CV of T-Nb_2O_5/3DNG, G) $NiCo_2S_4$, and H) SC T-Nb_2O_5/3DNG//$NiCo_2S_4$. A–H) Reproduced with permission.[84] Copyright 2020, Elsevier.

discharge states. In the first cycle, the embedding of Al^{3-} and Cl^- into Nb_2O_5 is relatively clear, but the disembedding process is not complete with remained original phase of Al and Cl. After two cycles, the crystal lattice still unchanged with intact tubular structure, showing excellent cyclic stability. It is worth mentioning that Nb_2O_5 nanotubes have high specific capacity and reversible stability at room temperature or even 50 °C in RAIB (**Figure 17**).

Nb-based materials also have good prospect in vanadium redox flow cells and fuel cells. However, it mainly plays a catalytic role in most of them, so this review only takes fuel cells as an example.

Fuel cells, including anode, cathode and electrolyte, convert chemical energy (such as hydrogen and methanol) to electrical energy through electrochemical reaction between positively charged protons and oxidizers (air or pure oxygen).,[89] and are regarded as pollution-free power source with higher energy efficiency and density compared with other conventional energy conversion systems.[90] At present, the fuel cells technology cannot meet the demand of mass promotion considering its high cost—precious metal on anode side, and relatively poor durability—slow oxygen reduction reaction on cathode side.[91] The existing means to solve aforementioned problem is to develop high-performance cathode materials with low-cost and nonprecious metals (**Figure 18**).

Zeng et al.[92] coated the continuous Pt thin membrane on the surface of Nb_2O_5 nanobelts (NBs) as catalyst support. The obtained Pt/Nb_2O_5 NBs was assembled into catalyst coating membrane (CCM) electrode by simple decal method. The resultant CCM has many advantages: 1) Ultra-thin and continuous catalyst layer alleviates Pt dissolution; 2) Vertically arranged pores facilitate mass transfer; 3) Catalyst layer does not need proton conduction ionizing polymers. In addition, the absence of carbon carrier eliminates concerns about carbon corrosion. Meanwhile, the catalyst layer's low curvature and the polymer removal help proton transport. Given the aforementioned advantages, the CCM has ultra-high durability and catalyst utilization ratio. In general, as for fuel cells, Nb-based materials mostly were used as load-supporting frameworks for catalyst by its chemical stability.

4. Modification and Optimization of Nb-Based Materials

4.1. Morphology Optimization

Different morphologies have a great influence on the exposure degree of active sites, the specific surface area of material, the accessibility of electrolyte and the electron transport path, which have been verified in electrochemical energy storage.[93] Development of nanotechnology provides an opportunity to design and construct favorable nano-morphologies. The three main characteristics of nanoscale materials are their small size, high specific surface area, and easy stress relaxation processes.[94]

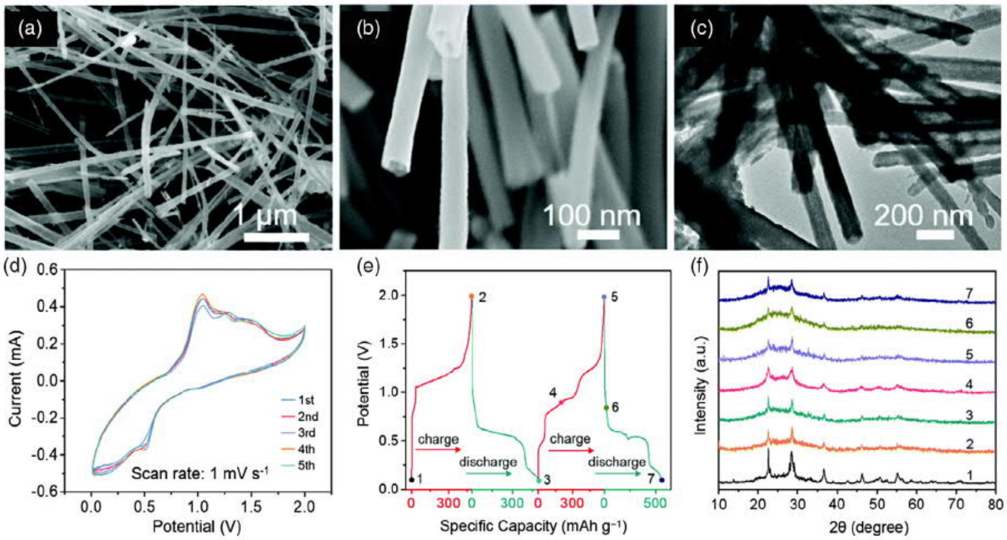

Figure 17. a,b) SEM, c) TEM, d) CV, e) GCD, and f) ex situ XRD patterns of the Nb_2O_5 nanotube. a–f) Reproduced with permission.[88] Copyright 2020, Royal Society of Chemistry.

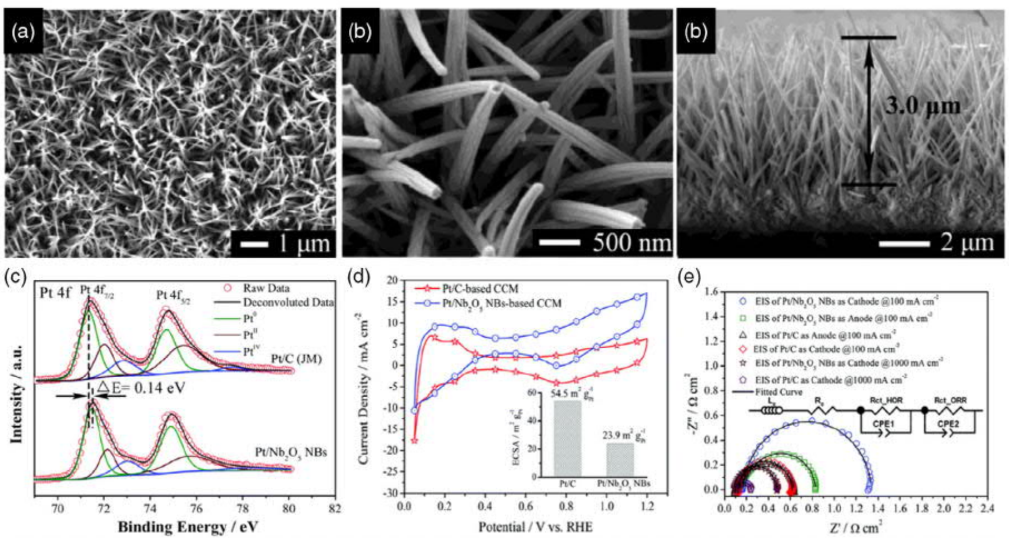

Figure 18. a–c) SEM, d) XPS, e) CV and f) EIS of Pt/Nb_2O_5 NBs. a–f) Reproduced with permission.[92] Copyright 2017, Royal Society of Chemistry.

The materials with particle sizes ranging from hundreds to tens of nanometers can effectively reduce ions diffusion path and greatly improve rate performance, which has been confirmed in Li/Na cell systems and polyvalent ion (such as Zn^{2+},[95] Mg^{2+},[96] and Al^{3+}[97]) cells. For example, Nb_2O_5 microsphere (about 12 nm), prepared by Lim et al.[98] through microemulsion method, offers high electrochemical activity and stability. Also, large specific surface area has a great impact on energy storage devices (especially SCs), which results in high-level charge storage from double layer and surface redox process.[99] In addition, it increases the contact area between electrodes and electrolytes, conducive to the utilization of electrochemical active surfaces. Meanwhile, the adaptability of stress relaxation is one of the important factors in morphology design of nanomaterials.[100] It is well known that the charge storage process of material is usually accompanied by volume expansion/contraction, leading to the crushing and rapid capacity attenuation.[1] The design of nanometer morphology is an effective method to enhance the stress-relaxation adaptability, such as the concept of nanocage.[101] By this optimized mode, some materials even approach the theoretical limit of electrochemical energy storage. Furthermore, various dimensional morphologies often have special properties. For example, interwoven 1D fiber materials are often used as flexible electrode materials. Liu and co-workers[102] synthesized multi-channel Nb_2O_5NRs/NMMCNF by electrostatic spinning, which not only has good flexible characteristics but also shows fast charge transfer kinetics. In this review, Nb-based materials of distinct dimensions will be summarized and described.

4.1.1. Zero-Dimension

As a low-dimensional material, zero-dimension (0D) is the first to appear and be used, such as 0D gold nanoparticle.[103] In general, 0D materials contain nanoparticle,[104] nanocrystalline,[105,106] and quantum dots,[107] etc, which have attracted much attention and research in the field of energy storage considering their advantages, such as small size, large specific surface area, and more exposed active points. However, its small size and abundant active sites on surface also make it prone to agglomeration.[108] Thus, it is a common design scheme to load 0D Nb-based materials on porous carbon materials, which can restrain the agglomeration and improve the poor conductivity. Zhou and co-workers[109] loaded Nb_2O_5 quantum dots (NQD–NC) on N-doped porous carbon derived from ZIF-8 for Li^+ hybrid capacitor. As described earlier, the addition of carbon enhance the conductivity of NQD–NC (about 47 Ω, far lower than the pure Nb_2O_5 (≈180 Ω)). The high surface area and advanced pore structure of carbon arised from metal–organic framework (MOF) are beneficial to enlarge ion transfer rate of reaction. The uniform distribution and immobilization of Nb_2O_5 quantum dots can provide large space to buffer the volume change during the cycle, achieving high cycle stability (retained 82% capacity after 3000 cycles). Also, its small size can shorten the length of Li^- and electron transfer, resulting in rapid charge transfer rate. One of the ways to prepare 0D quantum dots is to restrict the aggregation and particle growth of Nb using the advantage of multi-functional groups in biomass. For example, Lian et al.[110] used the chelating cooperation between egg white and Nb^{5-} to prepare Nb_2O_5 quantum dots embedded in biomass carbon by limiting its particle size growth during pyrolysis. Here, the quantum dots with small size offer more active sites, high energy density (67.2 Wh kg^{-1}) and power density (8750 W kg^{-1}) in Li^+ hybrid capacitor. Furthermore, the mosaic structure ensures its high cyclic stability (**Figure 19**).

The surface of 0D materials has a large number of active sites, which is beneficial for energy storage. But just this reason, it is easy to agglomerate, which usually leads to the instability of morphology and performance. The defects can be well suppressed by combining them with different phases.

4.1.2. One-Dimensional

One-dimensional (1D) nanomaterials have 2D directions in space, typically diameter in nanoscale and macroscopic in length. In general, the 1D nanomaterial has large length–diameter ratio, reaching up to several times or more. The most common 1D nanomaterial is carbon nanotubes, greatly promoting its research and application.[111,112] Afterward, many 1D nanomaterials have been prepared, such as nanorod,[102,113] nanowire,[114,115] NB,[116] etc. Because of the unique geometry characteristics, 1D nanomaterials can effectively accelerate charge transfer and inhibit agglomeration.[6] Its short diffusion length and good adaptability to large volume changes are also beneficial to energy storage, thus being of great application potential.[117] In addition, the flexible devices constructed by 1D materials are also the focus of research and application.

Many relatively mature approaches have been used to synthesize Nb-based nanomaterials with diverse porosity and internal structure, such as electrostatic spinning,[118] template-assisted method,[23] chemical deposition,[119] chemical etching,[120,121] etc. As for electrostatic spinning, polymer solutions or melts are sprayed into tiny jets in a strong electric field, and then solidified into 1D nanofibers after traveling considerable distance.[122] Wang and co-workers[123] prepared 1D nanofiber composite (M-Nb_2O_5/CNF) coated with Nb_2O_5 nanoparticles via electrostatic spinning. Nb_2O_5 nanoparticles in fiber shorten the electron/ion transport path and disperse the mechanical stress caused by volume expansion during energy storage. The long and thin mesoporous fiber have ultra-short diffusion paths for both sodium ions (Na^+) and electrons (e^-) along with more active sites, further ensuring sufficient contact between electroactive material and electrolyte. Second, polyacrylonitrile (PAN)-derived carbon as robust conductive network endows Nb_2O_5 with high conductivity. Finally, the independent nanofiber structure can maintain the structural integrity of M-Nb_2O_5/CNF and inhibit the volume strain and breakage during cycling process. Moreover, the flexibility of long fibers increases its applications range. This article reports its application in flexible Na^+ hybrid capacitor without current collector, showing good cycling stability (after 10 000 cycles, retained 94% capacity) and capacitance (287 mAh g^{-1} at 0.5 C). More importantly, due to the free-standing flexible electrode configuration, the M-Nb_2O_5/CNF//GF/mCNF NIC exhibits large volumetric energy and power densities (11.2 mWh cm^{-3}, 5.4 W cm^{-3}) based on the full device, which holds great promise in a wide variety of flexible electronics (**Figure 20**).

The template-assisted method is also one of the most commonly used strategy for morphology design and preparation.[124–126] The 1D template as growth matrix can maintain the dimension of material by sacrificing or retaining templates, whose choice is the key of study. For example, Zheng and co-workers[127] selected biomass fibro bacteria as growth matrix to load $Ti_2Nb_{10}O_{29}$. Furthermore, the influence rule of oxygen vacancy constructed by hydrogen reduction in LIB has been researched. DFT calculation and synchrotron radiation showed that the oxygen vacancy introduced on surface improved the electronic state of $Ti_2Nb_{10}O_{29}$ and reduced the bandgap of $Ti_2Nb_{10}O_{29-x}$. Hybridized elements (N, S, P, etc.) in biomass carbon (as conductive network) coupled with the oxygen vacancy of $Ti_2Nb_{10}O_{29-x}$ from inside to outside can construct fast ion/electron transport channel, and achieve high capacity (281 mAh g^{-1} at 5 C) and ultra-long cycle stability (after 500 cycles 94% were retained).

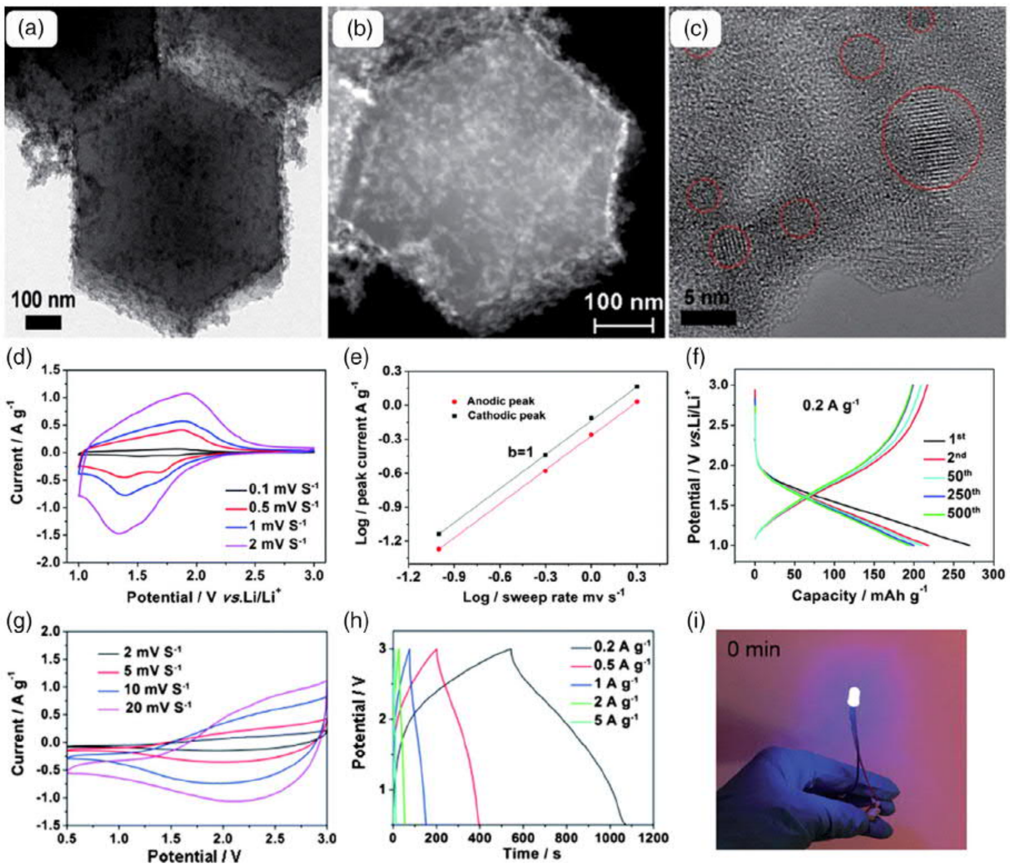

Figure 19. a) SEM and b,c) HRTEM, d) CV curves, e) specific peak current, and f) GCD of NQD–NC. g) CV curves at different scan rates between 2 and 20 mV s^{-1} and h) GCD profile of NQD–NC//AC SC. i) NQD–NC//AC device lighting up the LED. a–i) Reproduced with permission.[109] Copyright 2016, Royal Society of Chemistry.

As the preparation methods become more and more simple, many studies have focused on Nb-based 1D materials. Compared with 0D materials, the 1D materials maintain highly conductive correlation along the long axis and short ion-transport path in the diameter direction. The suitable design of pore and lattice transport channels is an important direction of 1D Nb-based materials development.

4.1.3. Two-Dimensional

Especially for the influence of graphene, 2D materials, with atomic or molecular thickness and large plane lengths—shortening the electron/ion diffusion path, have been paid great attention in energy storage.[128] In this regard, 2D Nb-based materials with large transverse size, controllable clearance, and abundant active sites are ideal energy storage materials.[129] However, they also have some problems, such as restack/aggregation of single layer and poor conductivity.[129,130] Accordingly, the layer spacing regulation and introduction of interlayer conductive material are main ways to mitigate these problems.[131]

Similarly, Nb-based sulfides with clear 2D lamellar structure also have the aforementioned defects. Yang and co-workers[132] designed and synthesized the sandwich NbS_2@S@IG composite material, consisted of iodine-doped graphene (IG) interlayered with NbS_2@S, and studied the interface interaction relationship between the ternary materials. The IG-encased sandwich structure provide interconnected conductive network. Again, layered NbS_2/IG supply point-to-point close contact with sulfur particles, which can effectively capture and absorb sulfur with ultra-high rate, and buffer the wide range of sulfur volume fluctuations during charging and discharging. Furthermore, from the accidental discovery, the insertion of active sulfur into NbS_2 interlayers can further improve the inherent conductivity and polarity. Being of these advantages, NbS_2@S@IG showed superior cyclic stability in Li-S (only 0.22% reduction after 2000 cycles at 20 C) (**Figure 21**).

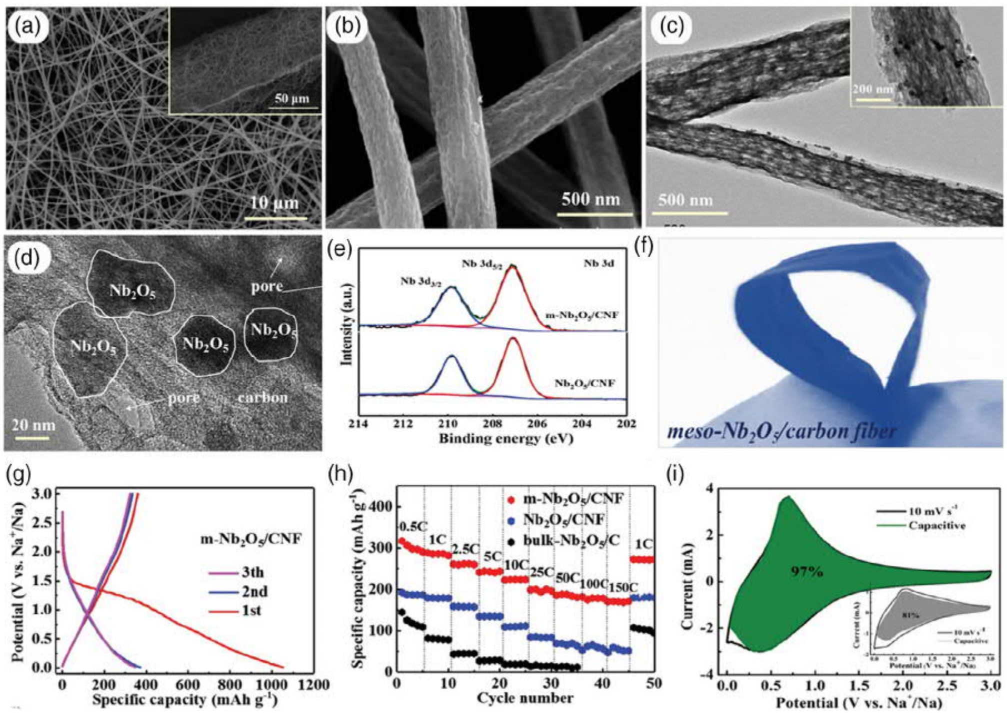

Figure 20. a,b) SEM images and c,d) HRTEM images of the m-Nb_2O_5/CNF. e) Nb3d peak of Nb_2O_5/CNF and m-Nb_2O_5/CNF. f) Photograph of m-Nb_2O_5/CNF. g) GCD curves of the m-Nb_2O_5/CNF electrode at 0.5 C within a potential range of 0.01–3 V versus Na/Na^- and h) Rate capability. i) Capacitive contribution curves of the m-Nb_2O_5/CNF at 10 mV s^{-1}. The inset in (i) is the capacitive contribution of Nb_2O_5/CNF. a–i) Reproduced with permission.[123] Copyright 2019, Wiley-VCH.

As well-known, Mxene, as relatively hot 2D layered material, is generally expressed as $M_{n-1}X_nT_x$, where T represents the surface-terminating group, such as O, F, OH, etc.[33] Mxene obtained by wet chemistry usually retains terminating groups on its surface, which enhance material hydrophilicity and offer high pseudocapacitance, together with its large specific surface area and metal conductivity (**Figure 22**a–i), showing excellent application prospect in SCs.[133] The Nb_4AlC_3 MAX phase, identified in 2007, has good thermal and electric conductivity, and large temperature stiffness, which makes Nb_4AlC_3 a promising candidate for high-temperature structural materials.[134] Again, $Nb_4C_3T_x$ from MAX phase also displays good conductivity and theoretical capacity for LIB.[135] Gogotsi and co-workers studied the changes rules of 2D $Nb_4C_3T_x$ microstructure and solid–liquid interface before and after cycles as LIB cathode.[136] After several cycles, the lattice and interlayer space of material are continuously enlarged, but its layer is not seriously pulverized due to the good rigidity. EIS tests at different potentials confirmed that SEI membrane formed below 1.2 V and dissolved off above 1.4 V. In addition, compared to other Mxene phases, $Nb_4C_3T_x$ exhibits smaller irreversible capacity during the first charge and discharge due to its better conductivity. Interestingly, its capacitance increased with the rise of cycle times (within 5000 cycles), ascribing to the enlarged accessibility of layer space for ion and gradually elevated stability of SEI membrane (Figure 22).

Nb-based materials can also be acquired by some special preparation methods, such as magnetron sputtering, electrochemical deposition, etc. In a word, due to the morphology advantages, most 2D Nb-based materials in energy storage have fast ion-transfer rate, good rate capability, and cycling stability. Also limited by its morphology, the 2D Nb-based materials have clear shortcomings, such as easy agglomeration and low conductive association between the sheets. Therefore, the prepared 2D materials often need further regulation and optimization to fully display their energy storage advantages.

4.1.4. Three Dimensional

3D materials in energy storage has a complex type of morphologies, most of which have irregular structure, such as 3D porous structures.[137] Meanwhile, it also has certain commonalities, such as high specific surface area, developed pore structure and interconnected conductive network, easy large-scale production, which make it a hot design direction in energy storage applications.[138]

Because of the poor electrical conductivity, most Nb-based materials are often coupled with 3D conductive networks to

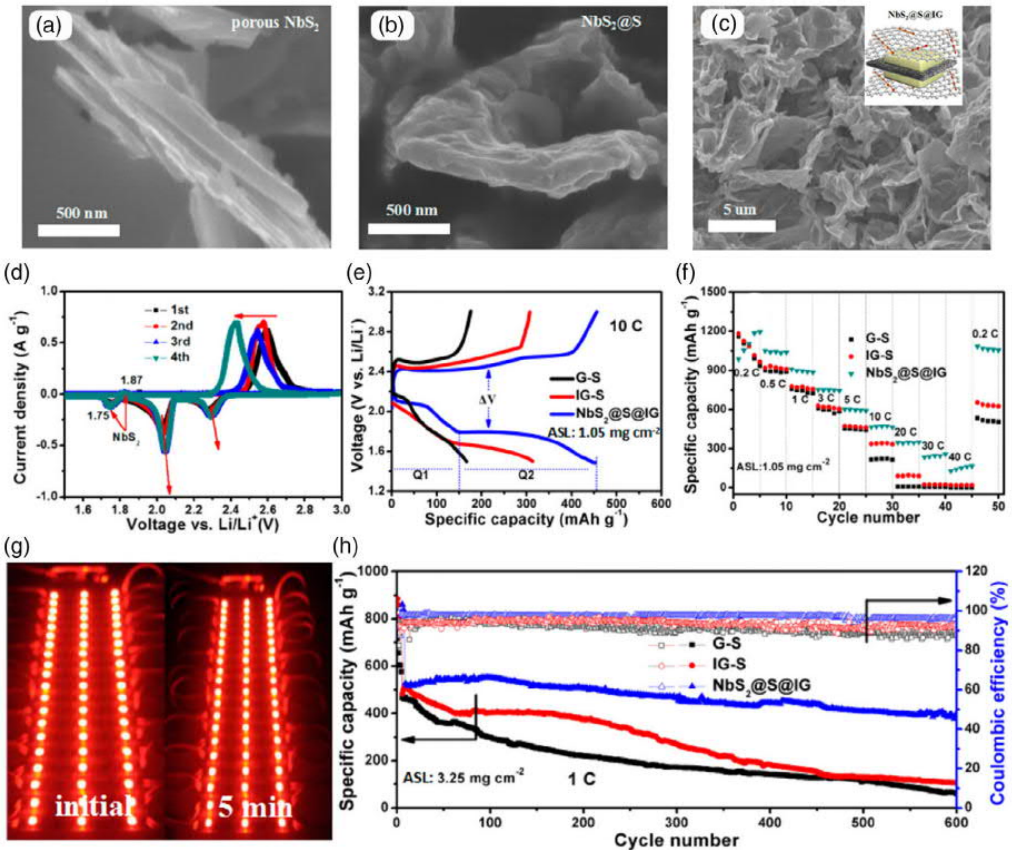

Figure 21. a) SEM of NbS_2, b) NbS_2@S, c) NbS_2@S@IG. d) CV profiles of NbS_2@S@IG electrode. e) Charge/discharge profiles of the first run at 10 C and f) rate performance profiles for G-S, IG-S, and NbS_2@S@IG electrodes. g) Digital photographs showing that three lithium batteries in series can light up 60 red indicators of 2835 LED modules. h) Cycling performance of NbS_2@S@IG electrode at 1 C with ASL of 3.25 mg cm^{-2}. a–h) Reproduced with permission.[132] Copyright 2017, American Chemical Society.

improve their energy storage performance. For example, Qin and co-workers[139] synthesized $Sn_2Nb_2O_7$/ SnO_2@3D carbon composite with self-buffering property by simple freeze-drying and carbonization method. This design mainly utilizes the small volume expansion ratio and fast ion diffusion rate of Nb_2O_5 in energy storage process to relieve the large volume expansion problem (520%) and the easy agglomeration phenomenon of Sn-based materials.[140] Here, 3D carbon mainly restrains the agglomeration of $Sn_2Nb_2O_7$/SnO_2 and enhances its electrical conductivity (**Figure 23a–i**). During the energy storage process, $Sn_2Nb_2O_7$ is transformed into Sn and $Na_xNb_2O_5$ on account of Na^+ insertion. It is worth noting that $Na_xNb_2O_5$ uniformly embedded in Sn can act as stable amorphous substrate to buffer the mechanical stress from Sn volume changes during subsequent Na^+ embedding/deembedding. In this unique structure, Sn/Nb-based materials achieve intelligent synergies with their synergy advantages. The 3D carbon network with excellent conductivity and capacitive behavior of M-$Sn_2Nb_2O_7$/ SnO_2@3DC can significantly improve electron and ion transport dynamics of the whole electrode (Figure 23).

Furthermore, the developed pore structure is also one of main purposes for 3D material design.[141] Sohn and co-workers[142] prepared Nb-doped TiO_2-C composite materials with 3D porous complex structure by hydrothermal-carbonization method. Due to the conductive graphite matrix and Nb-doped TiO_2 with metallic characteristics, the conductivity of composite material was largely enhanced. To be specific, Nb-doped TiO_2 nanocrystalline and conductive carbon can promote the Li^+ charge transfer, diffusion kinetics, and electron transport. Meanwhile, the substitution of different charge Nb^{5+} for Ti^{4+} can introduce additional carriers, thus improving the dynamics at different current densities. Nb-TiO_2-C has well-developed porous structure and controlled structural strain, which makes the volume change of Li^+ embedding/disembedding process effectively buffered. High conductivity and structural stability guarantee its excellent electrochemical capacity and cycling stability.

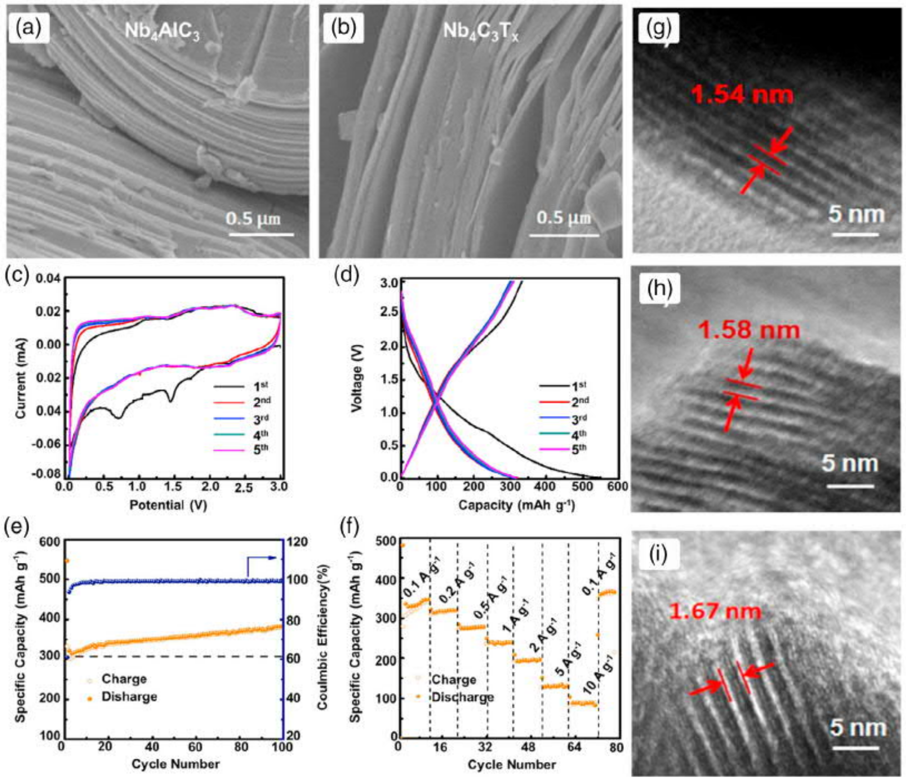

Figure 22. SEM of Nb_4AlC_3 and $Nb_4C_3T_x$, a) CV curves at a scan rate of 0.1 mV s^{-1}; b) Charge–discharge curves of $Nb_4C_3T_x$; c) Cycling performance at 100 mA g^{-1}; d) Capacity over cycling at different rates. HRTEM images of $Nb_4C_3T_x$ after a) 0, b) 160, and c) 1000 cycles, respectively. a–i) Reproduced with permission.[136] Copyright 2017, Elsevier.

4.1.5. Multistage Nanostructure

Under the synergistic effect of different low-dimension structures and large-size integrated particles, multistage nanostructures have great advantages in storage. In general, the low-dimensional configuration can promote electrons/ions transport, enlarge the contact area between electrodes and electrolyte. Also, high-dimensional configuration ensures structure stability and effectively alleviate the strain during repeated cycles.[59] The high-dimensional materials, although accumulated or constructed by low-dimensional materials usually with large gaps, have higher density and more perfect conductive network compared with the original scattered low-dimensional structures.

The common multistage nanostructures are the combination of "point-line-plane". Shu and co-workers[143] fabricated nanofibers (secondary morphology) consisted of $BaNb_{3.6}O_{10}$ nanoparticles (primary morphology) via electrospinning-annealing, showing flexible membrane structure (tertiary morphology) at macro level. The 1D nanofibers, being of single-crystal nanoparticles, have more exposed interfaces between electrolyte and electrode to shorten the diffusion path in the primary particles, thus achieve superior rate stability. In addition, $BaNb_{3.6}O_{10}$ nanofibers maintained their original shape well after a series of intense tensile tests, indicating its excellent stability and flexibility. Moreover, in situ characterization proved its low volume expansion ratio (5.9%) and high redox potential, unhelpful to the growth of lithium dendrites, both of which ensured its ultra-high cycle stability (retain >60% after 5000 cycles) and rate capability. The good tensile properties and cyclic stability are largely ascribed to the large gap between nanoparticles, which impose a direct effect on the multistage structure (**Figure 24**).

3D nanosphere constructed by low dimension also is of common multistage structure. For example, Liu et al.[144] synthesized porous $Ti_2Nb_{10}O_{29}$/C microspheres with interconnected nanoparticles by one-pot solvent-thermal method. Abundant pores and doped heteroatoms are retained among nanoparticles, conducive to the improvement of electrolyte infiltration, Li^+ diffusion coefficient and conductivity, thus achieving excellent Li^+ storage performance. This kind of morphological design has been widely recognized and developed.

In conclusion, the design of advanced morphology to optimize material electrochemical properties is one of the most reported

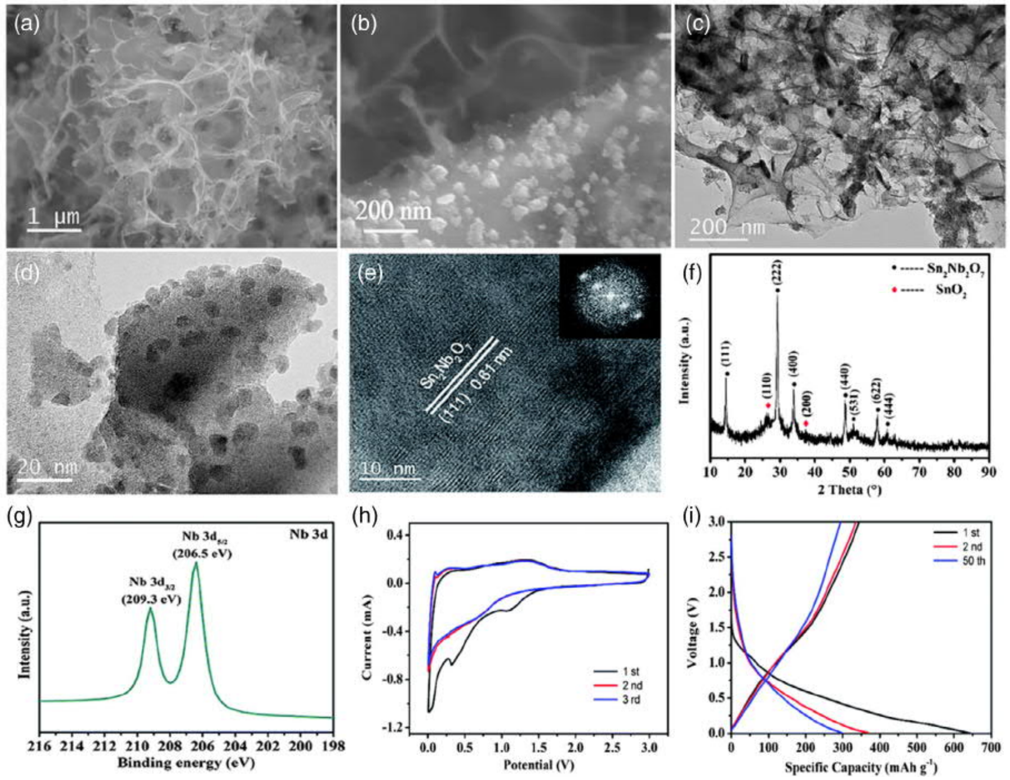

Figure 23. SEM, TEM, XRD, and XPS of M-$Sn_2Nb_2O_7/SnO_2$ @3DC. CV and GCD curves of the M-$Sn_2Nb_2O_7/SnO_2$@3DC electrode at a potential window of 0.005–3 V (vs Na^+/Na). a–f) Reproduced with permission.[139] Copyright 2017, Royal Society of Chemistry.

research directions. Different dimensional morphologies have their own advantages in energy storage. To pursue better electrochemical performance, the design of morphology has become more and more complex. For example, spheres morphologies have evolved from the original solid structure to the onion-like multi-layer one. Morphology design has begun to pay more attention to both high specific surface area and reasonable density instead of sacrificing volume energy density for high stability. To construct high-dimensional and density materials, the multilevel nanostructures is an effective design direction.

4.2. Lattice Optimization

Optimizing the lattice properties of materials is common way for designing energy storage materials, such as doping[145] and vacancy.[146] Usually, lattice modification can achieve high electron conductivity and/or ionic diffusion coefficient and/or low average particle size of active materials. 1) Both doping and vacancy can effectively introduce unpaired electrons into the crystal, thus improving material electrical conductivity.[147] 2) Doped ions of different sizes or generation of certain vacancy defects can change crystal cells structure, expand lattice channels, thus enhance ions diffusion coefficient.[148] 3) Doped ions can hinder grain growth, resulting in smaller average particle size than pure.[149] In previous reports, doping and vacancy has been studied in Nb-based materials.

4.2.1. Heteroatomic Modification

Cationic: Although Nb-based materials have many advantages in energy storage, their finite theoretical capacity and poor conductivity are the key factors limiting their development.[7] Doping cation with high theoretical capacity and charge carrier is effective approach to improve these disadvantages. Lin and co-workers[150] investigated the influence of different amounts of V doping on Li^+ transmission dynamics of $TiNb_2O_7$. The presence of NB—V and V—O valence bonds in Raman characterization confirmed the successful doping of V Meanwhile, XRD of $TiNb_{2-x}V_xO_7$ still maintains its original characteristic peak, but with low angle peak deviation, which proves that V-doping extends its crystal plane spacing without changing original phase structure. Meanwhile, V-doping enlarges Li^+ transport channel and ion transport rate, ensuring high ionic accessibility of internal material. In other words, V-doping is beneficial to activate the

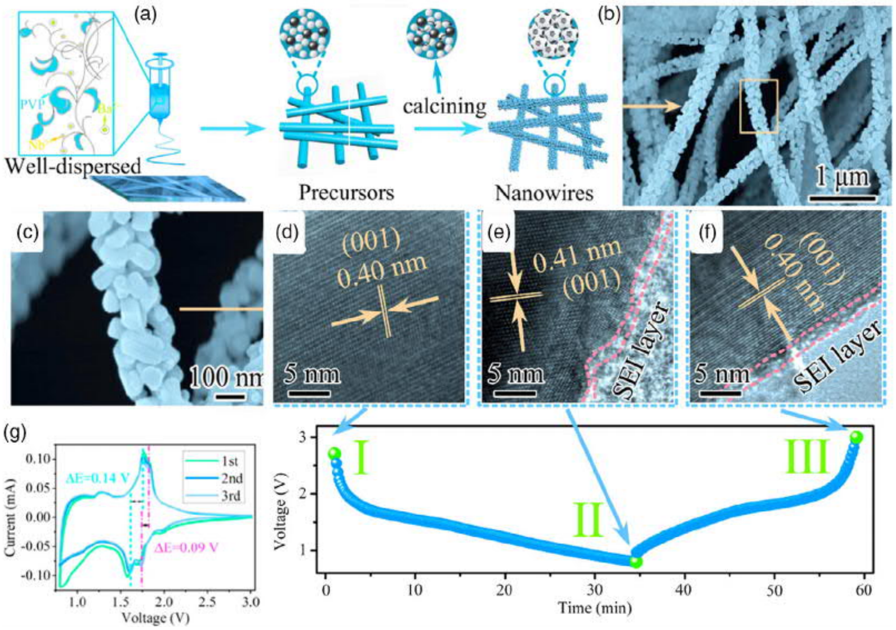

Figure 24. a) Schematic illustration of the formation of the synthesis of the $BaNb_{3.6}O_{10}$ nanowires through electrospinning. b,c) SEM, d–f) TEM and g) CV of $BaNb_{3.6}O_{10}$. Ex situ HRTEM of $BaNb_{3.6}O_{10}$ electrode. a–g) Reproduced with permission.[143] Copyright 2019, Elsevier.

inner part of material and improve its electrical capacity. In fact, compared with undoped $TiNb_2O_7$, V-doped sample capacity increased by more than 50 mAh g^{-1}.

On the other hand, self-doping (Nb) and even co-doping (Nb and heteroatom) are also effective means to improve its performance. Lin and co-workers[151] has conducted comprehensive study on co-doped with Cr^{3+} and Nb^{5+} double ions in $Ti_2Nb_{10}O_{29}$ (**Figure 25**a–g). Doped atoms changed the cell size and inhibited the growth of large particle size, along with the maintained typical Wadsley–Roth shear structure of $Ti_2Nb_{10}O_{29}$. Due to the increase in cell volume, the Li^+ diffusion coefficient of co-doped samples increased significantly. Meanwhile, the co-doped impurity bands largely improved material conductivity, proved by characterization and first principles calculations. Specifically, unpaired 3d electrons form Cr^{3+} with $t_{2g}^3e_g^0$ electronic configuration can enhance material conductivity. The size of Cr^{3+} (0.615 Å) and Nb^{5+}(0.64 Å) at octahedral position point, larger than that of Ti^{4+} (0.605 Å), leads to the increase in cell volume, helpful for the realization of greater Li^+ diffusion coefficient. In addition to cell morphology, the effect on particle size is also unneglectable. During calcination, the external Cr^{3+} effectively inhibits grain growth, beneficial to increase rate capability. In fact, compared with $Ti_2Nb_{10}O_{29}$, the conductivity and ionic diffusion coefficient (increasing by 8.2 times) of the doped samples were significantly improved in electrochemical tests (Figure 25).

Anion: Similar to cations, anions doping can also elevate materials properties, but often produce derivative vacancy structures. Xia and co-workers[152] grow N-doped $Ti_2Nb_{10}O_{29}$ in TiC/C-NC core branch skeleton to form heterogeneous structure array (N-TNO). Without changing raw materials morphology, N heteroatoms with symbiotic oxygen vacancy (confirmed by electron paramagnetic test) were doped via the thermal decomposition of melamine. By nitridation, some oxygen atoms in TNO lattice are replaced by nitrogen atoms, thus introducing more oxygen vacancies and producing new N 2p orbital above the valence band. The bandgap (*Eg*) of samples is calculated by UV–visible absorption spectra from the following equation

$$(\alpha h\nu)^2 = C(h\nu - E_g) \tag{7}$$

where C, $h\nu$, and α represent a coefficient, the energy of the scanning source light, and absorption coefficient, respectively. The direct effect of vacancy or doping defect on the bandgap can be quantified by this equation. Characterization confirmed the lower bandgap of N-TNO than that of TNO. Specifically speaking, N-doping and symbiotic oxygen vacancy can effectively improve the intrinsic electron conductivity, facilitate rapid electron and ion transfer. What is more, the TNO lattice expansion caused by doping broadens the Li^+ diffusion path, conducive to the rapid transmission (**Figure 26**).

Simultaneous optimization of Nb-based materials by anion and cation double doping is also one of the research directions. For example, Zong and co-workers[153] doped cations (such as iron (Fe), cobalt (Co), nickel (Ni)) and anions (such as selenium (Se)) in NbS_2 to explore their influence on the morphology and Li^+/Na^+ storage performance, and analyzes the energy storage mechanism of NbS_2 transformation into NbS and Nb

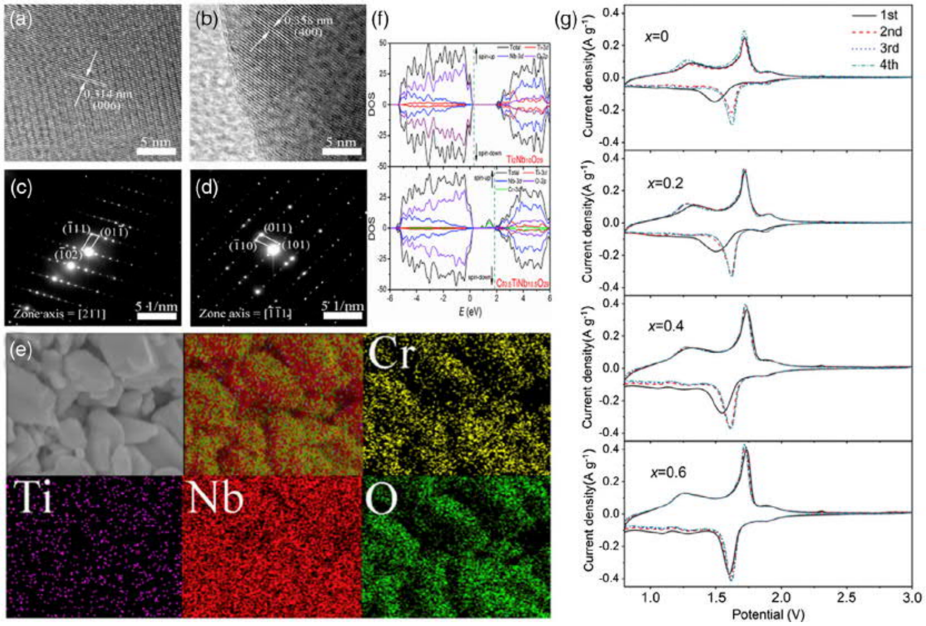

Figure 25. HRTEM images and SAED patterns of a,c) $Ti_2Nb_{10}O_{29}$ and b,d) $Cr_{0.6}Ti_{0.8}Nb_{10.6}O_{29}$. EDX elemental mapping image of $Cr_{0.6}Ti_{0.8}Nb_{10.6}O_{29}$. Calculated density of states (DOS) of $Cr_xTi_{2-2x}Nb_{10+x}O_{29}$ ($x = 0$ and 0.5). Fermi levels are indicated by dot lines. CV profiles of $Cr_xTi_{2-2x}Nb_{10+x}O_{29}$/Li ($x = 0$, 0.2, 0.4, and 0.6) cells at 0.1 mV s^{-1}. a–g) Reproduced with permission.[150] Copyright 2015, Elsevier.

during Li^+ embedding. Herein, the NbS_2 doped with Fe and Se showed the best electrochemical performance. Specifically, its nanometer morphology remained 2D on the whole, but its vertical and horizontal plane expanded with gradually uniform thickness (≈5 nm). Due to the addition of cation and anion, its capacitance increases greatly as well as good cycling stability. The abundant active sites and high specific surface area from even morphology integrated with good conductivity from hybrid lattices are the sources of excellent electrochemical properties (**Figure 27**).

4.2.2. Vacancy Modification

Incorporating atomic-scale defects, such as oxygen ion vacancies, into electrode materials is an effective strategy to improve the electrochemical performance of materials.[149] Vacancies can significantly change the oxide electronic structure or the adsorption intermediate stability, thereby greatly enhance the electrochemical activity of oxide surface.[148] Meanwhile, the vacancy structure will greatly affect material properties, such as electronic structure, conductivity, and ion/electron diffusion rate. In fact, the electronic properties adjusted by vacancies can effectively promote charge transfer and redox reaction kinetics.[154] The defects can also serve as additional insertion sites for inserting protons or cations to enable ion diffusion during electrochemical cycling.[155] In brief, these characteristics will improve electrochemical performance. In recent years, more and more attention has been paid to consciously introduce detects into the lattice structure of Nb-based materials.

The favorable role of oxygen vacancies in optimizing materials electrochemical activity has been recognized and studied. The small energy gap between the metal 3d and oxygen 2p band centers of TMOs can bring about strong covalent bonds, low charge transfers barrier, and outstanding electrochemistry performance. Lin and co-workers[12] prepared $Ti_2Nb_{10}O_{29-x}$ mesoporous microspheres and introduced O^{2} vacancy defects into shear-ReO_3 crystal structure by calcination to increase cell volume and Li^+ diffusion coefficient. XRD and XPS confirmed that oxygen vacancies and low valence Nb^{4+} (5.7% of all niobium atoms) were incorporated into TNO after calcination without affecting the crystal structure of ReO_3, just making the unit cell volume larger. Both $Ti_2Nb_{10}O_{29-x}$ and $Ti_2Nb_{10}O_{29}$ mesoporous microspheres showed abundant pore structure, and the introduction of vacancies did not affect the morphology and pore size distribution. Also, electrochemical tests have proved that the vacancies introduction did not change the basic mechanism of TNO electrochemical reaction, but improved its electrochemical kinetics. In addition to the oxygen vacancies generated by some materials calcining in oxygen-free environment, they can also be constructed on Nb-based materials by pyrolyzing carbon precursors. For example, Lian and co-workers[156] acquired the in situ vacant structure of $TiNb_2O_{7-x}$ nanochains by electrospinning. PAN pyrolysis and carbonization at high temperature would result in some vacancies in $TiNb_2O_7$ (verified by HRTEM and XPS (**Figure 28**)).

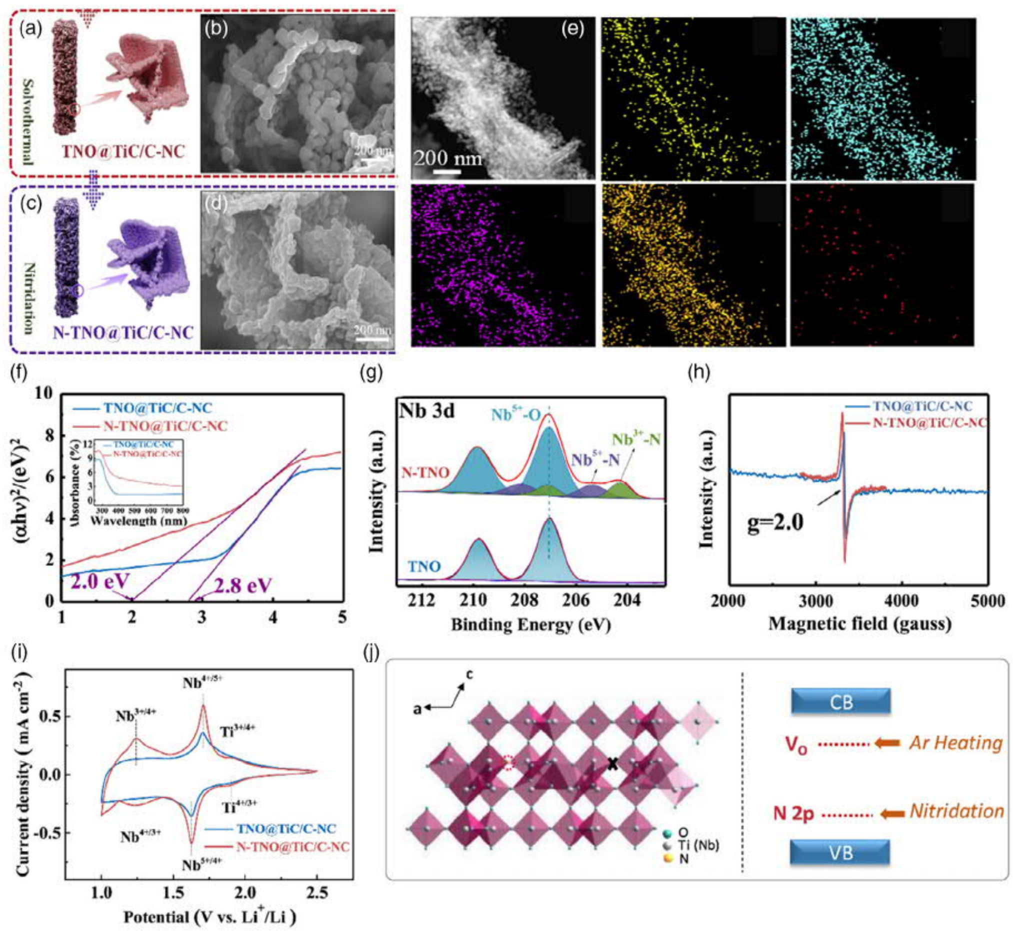

Figure 26. a,b) Schematic illustration and SEM images of TNO@TiC/C-NC and c,d) N-TNO@TiC/C-NC. e) Element mapping of N-TNO@TiC/C-NC composite. f) UV–vis absorption spectra, g) Nb 3d spectra, h) EPR spectrum, and i) CV cures of TNO@TiC/C-NC and N-TNO@TiC/C-NC. j) Crystal structure diagram and bandgap diagram of N-TNO. a–j) Reproduced with permission.[152] Copyright 2020, Elsevier.

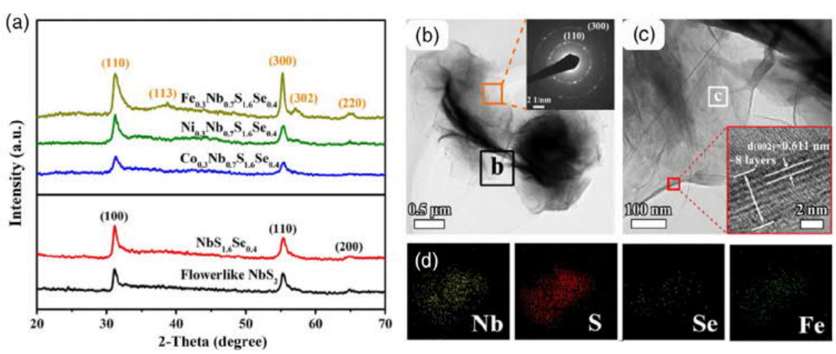

Figure 27. a) XRD of NbS_2-based nanosheets with different heteroatom doping. b) TEM image of $Fe_{0.3}Nb_{0.7}S_{1.6}Se_{0.4}$ nanosheets. Inset: SAED of the sample. c) Delicate image of (b). Inset: Layer of the sample. d) Mapping of $Fe_{0.3}Nb_{0.7}S_{1.6}Se_{0.4}$ nanosheets. a–f) Reproduced with permission.[153] Copyright 2017, American Chemical Society.

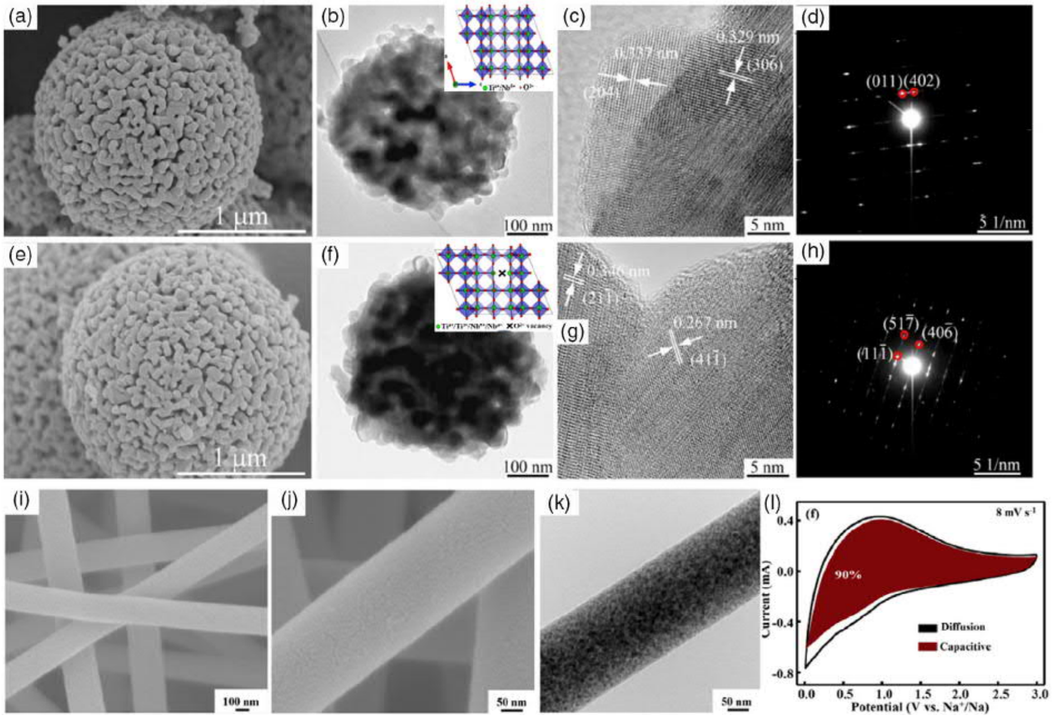

Figure 28. SEM and HRTEM of a–d) $Ti_2Nb_{10}O_{29}$ and e–h) $Ti_2Nb_{10}O_{29-x}$[12] i,j) SEM, k) TEM, and l) CV of S-Nb_2O_5@NS-PCNF. a–h) Reproduced with permission.[12] Copyright 2017, Elsevier. i–l) Reproduced with permission.[157] Copyright 2020, Elsevier.

Apart from calcination, the generation of oxidized vacancies by doping anions is also an effective approach for vacancy construction. For instance, Li and co-workers[157] obtained the vacancy structure by doping S anion in Nb_2O_5 and studies its variation rules in SIB. In this report, Nb_2O_5 quantum dots are embedded in CF with doped S (2.59 wt%) and N (3.24 wt%) elements, along with the existence of oxygen vacancy defects confirmed by XPS and Raman characterization. In the low-frequency region of the EIS test, the higher slope of S-Nb_2O_5@NS-PCNF represents its faster ion diffusion rate, proving the enhanced ion transmission by S-doping and vacancy structure. Similar, S-doping will generate more active sites due to the formation of a large number of oxygen vacancies and defects, sequentially achieving intensive conductivity and surface pseudocapacitance. Finally, electrochemical test of the assembled Na^+ capacitor also verified that S-Nb_2O_5@NS-PCNF has high energy density (112 Wh kg^{-1}), power density (7949 W kg^{-1}), and good cycling stability (retained 81% capacitance after 10 000 cycles).

4.3. Heterogeneous Collaborative Optimization

4.3.1. Metal Phase Coordination

Nb-based materials generally have relatively small volume changes in energy storage and fast ion transmission channels, but with limited capacity.[158] In contrast, metals, despite generally high theoretical capacity, has rapid capacitance decline due to the huge volume changes and lack of fast ion transport channels.[159] Therefore, their combination is also an effective measure to improve Nb-based materials. Yang and co-workers[160] produced synergic antimony–niobium pentoxide (Sb-Nb_2O_5) composite nanomesh through the decomposition of controllable $SbNbO_4$ nanosheet. Sb-Nb_2O_5, integrated the advantages of highly active Sb with stable structure of Nb_2O_5, shows enhanced charge transfer kinetics, large capacity, and high-rate Na^+ storage performance. Its XRD characterization corresponds to Sb (JCPDS 35-0732) and Nb_2O_5 (JCPDS 72-1297), rather than the new phase structure. The ultra-thin nanomesh, with lateral dimension of 1–5 µm and rough surface covered with 5–10 nm nanopores, can easily infiltrate the electrolyte and supply sufficient layered pathways for Na^+ diffusion to promote charge transfer dynamics. The well-dispersed monoclinic Nb_2O_5 nanoparticles in Sb–Nb_2O_5 nanomesh have fast surface control kinetics and stabilized structure during energy storage (**Figure 29**).

Chou[161] used polyoxyeboate precursor ($K_5[Cu(EN)_2]_{15.5}[(Nb_{24}O_{72}H_6)_2] \cdot 94.5H_2O$) as both Nb source and copper source to synthesize composite materials via hydrothermal-calcination. HRTEM observed that NbO/Cu (≈10 nm) grows on the surface of graphene oxide (GO), and the lattice also corresponds to NbO (0.24 nm) and Cu (0.21 nm). The unique nanoscale organic–inorganic hybrid crystals structure, based on polyoxamate (NbO/Cu nanoparticles are embedded in N-doped carbon

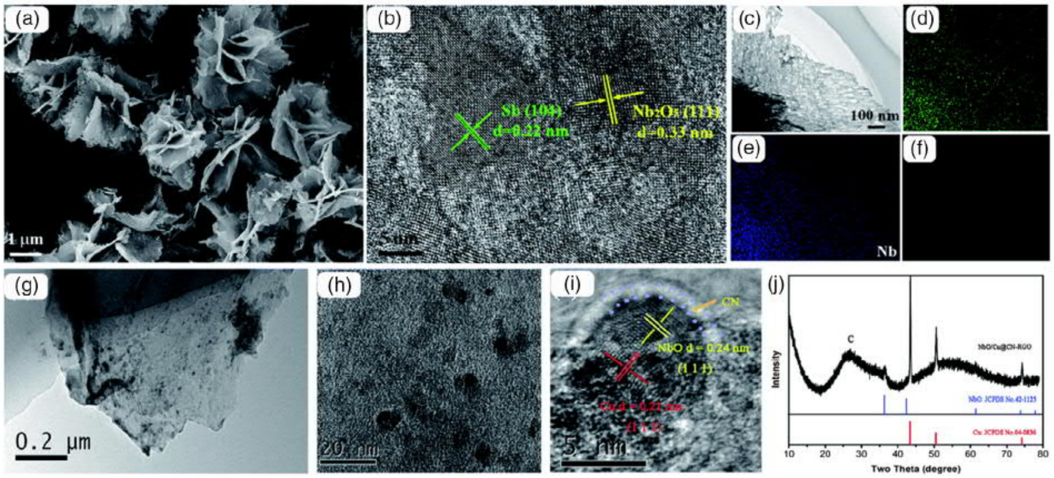

Figure 29. a) SEM, b) HRTEM, and c–f) mapping of Sb–Nb_2O_5.[160] g–i) HRTEM and j) XRD of NbO/Cu@NC-RGO.[161] a–f) Reproduced with permission.[160] Copyright 2018, Royal Society of Chemistry. g–i) Reproduced with permission.[161] Copyright 2019, Royal Society of Chemistry.

framework), can prevent the nanoparticles aggregation during heat treatment. The introduction of copper nanoparticles and reduced GO into new hybrid materials can promote electron transport and electrochemical reaction kinetics of NbO. These structural advantages allowed it to obtain impressive energy storage performance in subsequent Li^-/Na^+ devices.

The synergistic optimization effect between metal and niobium-based materials is similar to carbon composite. Yet metals tend to exhibit better bonding with Nb-based materials, and the valence bond relationship is closer. To date, the optimization mechanism of metal on niobium-based materials is not clear, and relative mechanism research is still lacking.

4.3.2. Carbon Synergy

The co-optimization of Nb-based materials by carbon phase has been drawn more attention. It is generally recognized that carbon materials can significantly improve the conductivity of Nb-based materials, as well as the solid–liquid interface stability, electron/ion transmission uniformity, and cycle stability of electrode materials in energy storage.[162] As described earlier, coating thin amorphous N-doped carbon layer on the surface of micron-level single-crystal H-Nb_2O_5 particles can eliminate the spatial and temporal desynchrony of Li^+ (de) intercalation from local inhomogeneity, and avoid the random phase transition of H-Nb_2O_5 crystal.[29] Except for the direct influence on the electrochemical performance of Nb-based materials, carbon-based materials are also common growth substrate for morphology design (such as carbon nanotubes,[163] carbon cloth, etc.). There are also many composite preparation methods, such as hydrothermal method, gel method, electrostatic spinning, and so on.[164] Compared with the metal phase, the direct valence bond relationship between carbon and niobium-based materials is less, mostly relying on the combination of heteroatom functional groups or defect structures on the surface of carbon phase.

4.4. Others

There are some more targeted optimization methods. In energy storage, the contact of Nb-based materials with electrolytes often leads to some unfavorable reactions, such as Nb-based materials dissolution and electrolytes decomposition. These irreversible reactions will hinder effective ion transport and reduce the durability of energy storage devices. In response to this problem, researchers modify the solid–liquid interface or coat the surface of niobium-based materials for protection.[165] The use of polymers or other thin layers to improve the interfacial stability is another research direction, but it mostly faces other phase materials, rather than changing the niobium.

5. Conclusion and Prospect

Nb-based materials, with high chemical stability, safe working potential and ideal electrical capacity, can be widely used in energy storage fields such as LIB, SIB, SC, Li–S, and fuel cells. Their excellent electrochemical performance (high capacitance of SC, excellent cycle and rate performance of LIB and SIB, and large corrosion resistance under actual fuel cell operating conditions) make them promising electrodes or supporting materials for widespread application in energy storage and conversion technologies. The main drawbacks of Nb-based materials are their rate capability restricted by their low conductivity and accessibility to electrons/ions in internal space. Therefore, designing different dimensional morphologies to shorten the ion transmission distance and increase the electrochemical reaction specific surface area, doping heteroatom, or importing vacancy structure to optimize lattice parameters and heterogeneous cooperative optimization to improve electronic conductivity and Li^+ diffusion coefficient are the key. In fact, Nb-based materials optimized by these three methods show good electrochemical performance. Nevertheless, there are still some problems in its practical application: 1) The morphology design with excellent performance often demands complicated or harsh experimental conditions, which makes it difficult to expand the production scale and meet commercial requirements. The morphology optimization has a huge effect on material performance, which has been widely recognized. Nonetheless, the preparation of special morphology often needs multi-step reactions, and the relatively harsh conditions (such as acid–base etching, high pressure and temperature, etc). Meanwhile, the factors such as high cost and safety in large-scale production also restrict its development. 2) The influence mechanism of lattice optimization (including doping and vacancy) on its doped elements and vacancy structure has not formed a rounded system. Despite many studies in this direction, the overall situation is chaotic with numerous and irregular doped elements. The influence of element differences (element diameter, charge amount, etc.) on doping optimization has not been confirmed in a systematic way. 3) Research on the relationship between the nanostructure of Nb-based materials and its electrochemical behavior (such as charge transfer and ion diffusion kinetics at electrode/electrolyte interface) is still not comprehensive enough to enable optimize material properties. 4) The high cost of Nb-based materials is also a limiting factor for its development and application. Efficient purification and recovery of Nb sources are the prerequisites for its development.

Hence, the development of simple and effective morphology design schemes and perfect optimization mechanisms are still important targets in Nb-based materials research.

Acknowledgements

This work was financially supported by Postgraduate Research & Practice Innovation Program of Jiangsu Province (grant number KYCX19_2101) and Natural Science Foundation of Shandong Province, China (grant number ZR2017MEM019).

Conflict of Interest

The authors declare no conflict of interest.

Keywords

battery systems, dimensionality, energy storage, Nb-based materials, vacancies

Received: September 4, 2020
Revised: October 2, 2020
Published online: October 28, 2020

[1] Q. Wu, R. Zhao, W. Liu, X. Zhang, X. Shen, W. Li, G. Diao, M. Chen, *J. Power Sources* **2017**, *344*, 74.
[2] Q. Ma, F. Tietz, *ChemElectroChem* **2020**, *7*, 2693.
[3] X. Yang, A. L. Rogach, *Adv. Energy Mater.* **2020**, *10*, 2000288.
[4] P. Geng, S. Cao, X. Guo, J. Ding, S. Zhang, M. Zheng, H. Pang, *J. Mater. Chem. A* **2019**, *7*, 19465.
[5] S. Zheng, H. Xue, H. Pang, *Coord. Chem. Rev.* **2018**, *373*, 2.
[6] G. Zhang, X. Xiao, B. Li, P. Gu, H. Xue, H. Pang, *J. Mater. Chem. A* **2017**, *5*, 8155.
[7] C. Nico, T. Monteiro, M. P. F. Graça, *Prog. Mater. Sci.* **2016**, *80*, 1.
[8] Q. Deng, Y. Fu, C. Zhu, Y. Yu, *Small* **2019**, *15*, 1804884.
[9] X. Guo, S. Zheng, G. Zhang, X. Xiao, X. Li, Y. Xu, H. Xue, H. Pang, *Energy Storage Mater.* **2017**, *9*, 150.
[10] L. Yan, X. Rui, G. Chen, W. Xu, G. Zou, H. Luo, *Nanoscale* **2016**, *8*, 8443.
[11] L. Wang, X. Bi, S. Yang, *Adv. Mater.* **2016**, *28*, 7672.
[12] S. Deng, Z. Luo, Y. Liu, X. Lou, C. Lin, C. Yang, H. Zhao, P. Zheng, Z. Sun, J. Li, N. Wang, H. Wu, *J. Power Sources* **2017**, *362*, 250.
[13] D. Music, S. Prünte, P. Keuter, A. Saksena, *J. Phys. D. Appl. Phys.* **2020**, *53*, 285303.
[14] C. Nico, M. R. N. Soares, J. Rodrigues, M. Matos, R. Monteiro, M. P. F. Graça, M. A. Valente, F. M. Costa, T. Monteiro, *J. Phys. Chem. C* **2011**, *115*, 4879.
[15] J. Li, W.-W. Liu, H.-M. Zhou, Z.-Z. Liu, B.-R. Chen, W.-J. Sun, *Rare Met.* **2018**, *37*, 118.
[16] S. Nakao, H. Kamisaka, Y. Hirose, T. Hasegawa, *Phys. status solidi* **2017**, *214*, 1600604.
[17] Y.-S. Kim, Y. Cho, P. M. Nogales, S.-K. Jeong, *Energies* **2019**, *12*, 2960.
[18] C. M. Fang, M. A. van Huis, Q. Xu, R. J. Cava, H. W. Zandbergen, *J. Mater. Chem. C* **2015**, *3*, 651.
[19] R. Li, X. Zhu, Q. Fu, G. Liang, Y. Chen, L. Luo, M. Dong, Q. Shao, C. Lin, R. Wei, Z. Guo, *Chem. Commun.* **2019**, *55*, 2493.
[20] R. Li, Y. Qin, X. Liu, L. Yang, C. Lin, R. Xia, S. Lin, Y. Chen, J. Li, *Electrochim. Acta* **2018**, *266*, 202.
[21] X. Chen, T. Yu, X. Fan, H. Zhang, Z. Li, J. Ye, Z. Zou, *Appl. Surf. Sci.* **2007**, *253*, 8500.
[22] L. Yang, Y.-E. Zhu, J. Sheng, F. Li, B. Tang, Y. Zhang, Z. Zhou, *Small* **2017**, *13*, 1702588.
[23] Y. Lian, D. Wang, S. Hou, C. Ban, J. Zhao, H. Zhang, *Electrochim. Acta* **2020**, *330*, 135204.
[24] X. Wang, C. Yan, J. Yan, A. Sumboja, P. S. Lee, *Nano Energy* **2015**, *11*, 765.
[25] S. Hemmati, G. Li, X. Wang, Y. Ding, Y. Pei, A. Yu, Z. Chen, *Nano Energy* **2019**, *56*, 118.
[26] L. Kong, X. Cao, J. Wang, W. Qiao, L. Ling, D. Long, *J. Power Sources* **2016**, *309*, 42.
[27] L. Kong, C. Zhang, J. Wang, W. Qiao, L. Ling, D. Long, *ACS Nano* **2015**, *9*, 11200.
[28] S. Fu, Q. Yu, Z. Liu, P. Hu, Q. Chen, S. Feng, L. Mai, L. Zhou, *J. Mater. Chem. A* **2019**, *7*, 11234.
[29] Z. Song, H. Li, W. Liu, H. Zhang, J. Yan, Y. Tang, J. Huang, H. Zhang, X. Li, *Adv. Mater.* **2020**, *32*, 2001001.
[30] X. Ou, X. Xiong, F. Zheng, C. Yang, Z. Lin, R. Hu, C. Jin, Y. Chen, M. Liu, *J. Power Sources* **2016**, *325*, 410.
[31] N. Wu, Z. Yang, W. Zhou, H. Zou, X. Xiong, Y. Chen, F. Ouyang, *J. Appl. Phys.* **2015**, *118*, 084306.
[32] R. Bianco, I. Errea, L. Monacelli, M. Calandra, F. Mauri, *Nano Lett.* **2019**, *19*, 3098.
[33] J. Yang, W. Bao, P. Jaumaux, S. Zhang, C. Wang, G. Wang, *Adv. Mater. Interfaces* **2019**, *6*, 1802004.
[34] Q. H. Nguyen, H. Kim, I. T. Kim, W. Choi, J. Hur, *Chem. Eng. J.* **2020**, *382*, 122981.
[35] L. Shi, Y. Gu, L. Chen, Z. Yang, J. Ma, Y. Qian, *Carbon N. Y.* **2005**, *43*, 211.
[36] S. Shen, X. Xia, Y. Zhong, S. Deng, D. Xie, B. Liu, Y. Zhang, G. Pan, X. Wang, J. Tu, *Adv. Mater.* **2019**, *31*, 1900009.
[37] W. Cai, G. Li, K. Zhang, G. Xiao, C. Wang, K. Ye, Z. Chen, Y. Zhu, Y. Qian, *Adv. Funct. Mater.* **2018**, *28*, 1704865.
[38] R. Liu, W. Cao, D. Han, Y. Mo, H. Zeng, H. Yang, W. Li, *J. Alloys Compd.* **2019**, *793*, 505.

[39] H. Zhang, J. Liu, Z. Tian, Y. Ye, Y. Cai, C. Liang, K. Terabe, *Carbon N. Y.* **2016**, *100*, 590.
[40] C. Dong, X. Wang, X. Liu, X. Yuan, W. Dong, H. Cui, Y. Duan, F. Huang, *RSC Adv.* **2016**, *6*, 81290.
[41] E. C. Ethridge, S. C. Erwin, W. E. Pickett, *Phys. Rev. B* **1996**, *53*, 12563.
[42] H. Shen, B. Wei, D. Zhang, Z. Qi, Z. Wang, *Mater. Lett.* **2018**, *229*, 17.
[43] V. I. Ivashchenko, P. E. A. Turchi, E. I. Olifan, *Phys. Rev. B* **2010**, *82*, 054109.
[44] K. R. Babu, G.-Y. Guo, *Phys. Rev. B* **2019**, *99*, 104508.
[45] X. Li, B. Gao, X. Huang, Z. Guo, Q. Li, X. Zhang, P. K. Chu, K. Huo, *ACS Appl. Mater. Interfaces* **2019**, *11*, 2961.
[46] W. Qiu, C. An, Y. Yan, J. Xu, Z. Zhang, W. Guo, Z. Wang, Z. Zheng, Z. Wang, Q. Deng, J. Li, *J. Power Sources* **2019**, *423*, 98.
[47] X.-P. Gao, H.-X. Yang, *Energy Environ. Sci.* **2010**, *3*, 174.
[48] Q. Fu, X. Zhu, R. Li, G. Liang, L. Luo, Y. Chen, Y. Ding, C. Lin, K. Wang, X. S. Zhao, *Energy Storage Mater.* **2020**, *30*, 401.
[49] R. Tao, G. Yang, E. C. Self, J. Liang, J. R. Dunlap, S. Men, C. Do-Thanh, J. Liu, Y. Zhang, S. Zhao, H. Lyu, A. P. Sokolov, J. Nanda, X. Sun, S. Dai, *Small* **2020**, *2001884*, 2001884.
[50] H. Lyu, J. Li, T. Wang, B. P. Thapaliya, S. Men, C. J. Jafta, R. Tao, X.-G. Sun, S. Dai, *ACS Appl. Energy Mater.* **2020**, *3*, 5657.
[51] R. S. Roth, L. W. Coughanour, *J. Res. Natl. Bur. Stand. (1934).* **1955**, *55*, 209.
[52] J.-J. Yang, Y.-R. Kim, M.-G. Jeong, Y.-J. Yuk, H.-J. Kim, S.-G. Park, *J. Electrochem. Sci. Technol.* **2015**, *6*, 59.
[53] B. Guo, X. Yu, X.-G. Sun, M. Chi, Z.-A. Qiao, J. Liu, Y.-S. Hu, X.-Q. Yang, J. B. Goodenough, S. Dai, *Energy Environ. Sci.* **2014**, *7*, 2220.
[54] H. Yu, X. Cheng, H. Zhu, R. Zheng, T. Liu, J. Zhang, M. Shui, Y. Xie, J. Shu, *Nano Energy* **2018**, *54*, 227.
[55] M. A. Reddy, U. V. Varadaraju, *J. Power Sources* **2006**, *159*, 336.
[56] S. Dong, Y. Zhou, C. Hai, J. Zeng, Y. Sun, Y. Shen, X. Li, X. Ren, C. Sun, G. Zhang, Z. Wu, *J. Power Sources* **2020**, *462*, 228185.
[57] M. Zheng, H. Tang, Q. Hu, S. Zheng, L. Li, J. Xu, H. Pang, *Adv. Funct. Mater.* **2018**, *28*, 1707500.
[58] J. B. Goodenough, *Energy Storage Mater.* **2015**, *1*, 158.
[59] Y. Shi, X. Pan, B. Li, M. Zhao, H. Pang, *Chem. Eng. J.* **2018**, *343*, 427.
[60] X. Cheng, H. Zhu, H. Yu, W. Ye, R. Zheng, T. Liu, N. Peng, M. Shui, J. Shu, *J. Mater. Chem. A* **2018**, *6*, 8620.
[61] Y. Zhu, J. G. Connell, S. Tepavcevic, P. Zapol, R. Garcia-Mendez, N. J. Taylor, J. Sakamoto, B. J. Ingram, L. A. Curtiss, J. W. Freeland, D. D. Fong, N. M. Markovic, *Adv. Energy Mater.* **2019**, *9*, 1803440.
[62] Y. Wang, D. Su, C. Wang, G. Wang, *Electrochem. commun.* **2013**, *29*, 8.
[63] J. Ni, W. Wang, C. Wu, H. Liang, J. Maier, Y. Yu, L. Li, *Adv. Mater.* **2017**, *29*, 1605607.
[64] X. Tang, D. Zhou, P. Li, X. Guo, B. Sun, H. Liu, K. Yan, Y. Gogotsi, G. Wang, *Adv. Mater.* **2020**, *32*, 1906739.
[65] B. Cao, Q. Zhang, H. Liu, B. Xu, S. Zhang, T. Zhou, J. Mao, W. K. Pang, Z. Guo, A. Li, J. Zhou, X. Chen, H. Song, *Adv. Energy Mater.* **2018**, *8*, 1801149.
[66] J.-Y. Hwang, S.-T. Myung, Y.-K. Sun, *Adv. Funct. Mater.* **2018**, *28*, 1802938.
[67] H. Sun, L. Mei, J. Liang, Z. Zhao, C. Lee, H. Fei, M. Ding, J. Lau, M. Li, C. Wang, X. Xu, G. Hao, B. Papandrea, I. Shakir, B. Dunn, Y. Huang, X. Duan, *Science (80-.).* **2017**, *356*, 599.
[68] Z. Tong, R. Yang, S. Wu, D. Shen, T. Jiao, K. Zhang, W. Zhang, C. Lee, *Small* **2019**, *15*, 1901272.
[69] A. Henry, S. Le Vot, J. G. Alauzun, P. Hesemann, M. L. Foresti, P. Cerruti, L. Heux, O. Fontaine, B. Boury, *Electrochim. Acta* **2019**, *313*, 478.
[70] N. Li, F. Zhang, Y. Tang, *J. Mater. Chem. A* **2018**, *6*, 17889.
[71] D. Su, D. Zhou, C. Wang, G. Wang, *Adv. Funct. Mater.* **2018**, *28*, 1800154.
[72] M. Wadman, *Science* **2018**, *359*, 13.
[73] Z. Wu, W. Wang, Y. Wang, C. Chen, K. Li, G. Zhao, C. Sun, W. Chen, L. Ni, G. Diao, *Electrochim. Acta* **2017**, *224*, 527.
[74] W. Li, R. Zhao, K. Zhou, C. Shen, X. Zhang, H. Wu, L. Ni, H. Yan, G. Diao, M. Chen, *J. Mater. Chem. A* **2019**, *7*, 8443.
[75] T. Tao, S. Lu, Y. Fan, W. Lei, S. Huang, Y. Chen, **2017**, *1700542*, 1.
[76] D. Luo, Z. Zhang, G. Li, S. Cheng, S. Li, J. Li, R. Gao, M. Li, S. Sy, Y.-P. Deng, Y. Jiang, Y. Zhu, H. Dou, Y. Hu, A. Yu, Z. Chen, *ACS Nano* **2020**, *14*, 4849.
[77] H. Li, Z. Ge, Y. Zheng, Y. Xue, G. Bai, J. Wang, K. Zhuo, Y. Wang, *Chem. Commun.* **2019**, *55*, 1991.
[78] A. A. Lubimtsev, P. R. C. Kent, B. G. Sumpter, P. Ganesh, *J. Mater. Chem. A* **2013**, *1*, 14951.
[79] K. Naoi, S. Ishimoto, J. Miyamoto, W. Naoi, *Energy Environ. Sci.* **2012**, *5*, 9363.
[80] H. Wang, C. Zhu, D. Chao, Q. Yan, H. J. Fan, *Adv. Mater.* **2017**, *29*, 1702093.
[81] X. Wang, G. Shen, *Nano Energy* **2015**, *15*, 104.
[82] B. Li, J. Zheng, H. Zhang, L. Jin, D. Yang, H. Lv, C. Shen, A. Shellikeri, Y. Zheng, R. Gong, J. P. Zheng, C. Zhang, *Adv. Mater.* **2018**, *30*, 1705670.
[83] Y. Yan, B. Li, W. Guo, H. Pang, H. Xue, *J. Power Sources* **2016**, *329*, 148.
[84] M. Zhang, H. Liu, Z. Song, T. Ma, J. Xie, *Chem. Eng. J.* **2020**, *392*, 123669.
[85] Y. Ru, S. Zheng, H. Xue, H. Pang, *J. Mater. Chem. A* **2019**, *7*, 14391.
[86] Q. Zhou, D. Wang, Y. Lian, S. Hou, C. Ban, Z. Wang, J. Zhao, H. Zhang, *Electrochim. Acta* **2020**, *354*, 136677.
[87] S. Lee, J. Cho, *Angew. Chemie Int. Ed.* **2015**, *54*, 9452.
[88] L. Wang, H. Lin, W. Kong, Y. Hu, R. Chen, P. Zhao, M. Shokouhimehr, X. L. Zhang, Z. Tie, Z. Jin, *Nanoscale* **2020**, *12*, 12531.
[89] R. Dutta, A. Maity, A. Marsicano, M. Ceretti, D. Chernyshov, A. Bosak, A. Villesuzanne, G. Roth, G. Perversi, W. Paulus, *J. Mater. Chem. A* **2020**, *8*, 13987.
[90] K. Asazawa, K. Yamada, H. Tanaka, A. Oka, M. Taniguchi, T. Kobayashi, *Angew. Chemie Int. Ed.* **2007**, *46*, 8024.
[91] Z. Du, K. Li, H. Zhao, X. Dong, Y. Zhang, K. Świerczek, *J. Mater. Chem. A* **2020**, *8*, 14162.
[92] Y. Zeng, X. Guo, Z. Wang, J. Geng, H. Zhang, W. Song, H. Yu, Z. Shao, B. Yi, *Nanoscale* **2017**, *9*, 6910.
[93] G. Longoni, M. Fiore, J.-H. Kim, Y. H. Jung, D. K. Kim, C. M. Mari, R. Ruffo, *J. Power Sources* **2016**, *332*, 42.
[94] A. Mukherjee, T. Sharabani, R. Sharma, S. Okashy, M. Noked, *Batter. Supercaps* **2020**, *3*, 510.
[95] Z. Yuan, Y. Yin, C. Xie, H. Zhang, Y. Yao, X. Li, *Adv. Mater.* **2019**, *31*, 1902025.
[96] Q. D. Truong, M. K. Devaraju, I. Honma, *J. Power Sources* **2017**, *361*, 195.
[97] H. Yang, H. Li, J. Li, Z. Sun, K. He, H. Cheng, F. Li, *Angew. Chemie Int. Ed.* **2019**, *58*, 11978.
[98] E. Lim, C. Jo, H. Kim, M.-H. Kim, Y. Mun, J. Chun, Y. Ye, J. Hwang, K.-S. Ha, K. C. Roh, K. Kang, S. Yoon, J. Lee, *ACS Nano* **2015**, *9*, 7497.
[99] S. Hou, Y. Lian, Y. Bai, Q. Zhou, C. Ban, Z. Wang, J. Zhao, H. Zhang, *Electrochim. Acta* **2020**, *341*, 136053.
[100] B. Peng, Z. Sun, S. Jiao, G. Wang, G. Zhang, *Batter. Supercaps* **2020**, *3*, 147.
[101] X. Zhang, R. Zhao, Q. Wu, W. Li, C. Shen, L. Ni, H. Yan, G. Diao, M. Chen, *ACS Nano* **2017**, *11*, 8429.

[102] L. She, F. Zhang, C. Jia, L. Kang, Q. Li, X. He, J. Sun, Z. Lei, Z.-H. Liu, *J. Colloid Interface Sci.* **2020**, *573*, 1.
[103] S. Rakshit, S. P. Moulik, S. C. Bhattacharya, *J. Colloid Interface Sci.* **2017**, *491*, 349.
[104] Q. Tian, Y. Chen, F. Zhang, W. Zhang, Z. Sui, L. Yang, *Appl. Surf. Sci.* **2020**, *511*, 145625.
[105] R. Alcántara, G. Ortiz, I. Rodríguez, J. L. Tirado, *J. Power Sources* **2009**, *189*, 309.
[106] M. Zou, W. Wen, J. Li, Y. Lin, H. Lai, Z. Huang, *J. Energy Chem.* **2014**, *23*, 513.
[107] P. Wu, Y. Xu, J. Zhan, Y. Li, H. Xue, H. Pang, *Small* **2018**, *14*, 1801479.
[108] Y. Li, J. Yang, J. Song, *Renew. Sustain. Energy Rev.* **2016**, *65*, 685.
[109] S. Liu, J. Zhou, Z. Cai, G. Fang, Y. Cai, A. Pan, S. Liang, *J. Mater. Chem. A* **2016**, *4*, 17838.
[110] Y. Lian, Z. Xu, D. Wang, Y. Bai, C. Ban, J. Zhao, H. Zhang, *J. Alloys Compd.* **2021**, *850*, 156808.
[111] Q. Wu, R. Xu, R. Zhao, X. Zhang, W. Li, G. Diao, M. Chen, *Energy Storage Mater.* **2019**, *19*, 69.
[112] W. Chen, Z. Zhao, X. Yu, *Electrochim. Acta* **2020**, *341*, 136044.
[113] Q. Fu, X. Liu, J. Hou, Y. Pu, C. Lin, L. Yang, X. Zhu, L. Hu, S. Lin, L. Luo, Y. Chen, *J. Power Sources* **2018**, *397*, 231.
[114] Y. Li, R. Zheng, H. Yu, X. Cheng, T. Liu, N. Peng, J. Zhang, M. Shui, J. Shu, *ACS Appl. Mater. Interfaces* **2019**, *11*, 22429.
[115] X. Wang, Q. Li, L. Zhang, Z. Hu, L. Yu, T. Jiang, C. Lu, C. Yan, J. Sun, Z. Liu, *Adv. Mater.* **2018**, *30*, 1800963.
[116] H. Zhu, L. Yan, M. Xia, X. Cheng, W. Ye, H. Yu, N. Long, M. Shui, J. Shu, *J. Power Sources* **2019**, *426*, 250.
[117] Q. Zhao, M. Zhao, J. Qiu, W.-Y. Lai, H. Pang, W. Huang, *Small* **2017**, *13*, 1701091.
[118] S.-Y. Jang, V. Seshadri, M.-S. Khil, A. Kumar, M. Marquez, P. T. Mather, G. A. Sotzing, *Adv. Mater.* **2005**, *17*, 2177.
[119] K. Wen, W. He, *Nanotechnology* **2015**, *26*, 382001.
[120] R. Chu, D. Tan, J. Zhang, Y. Chen, H. Jiang, J. Lin, L. Li, Y. Zhang, H. Guo, *J. Alloys Compd.* **2020**, *835*, 155192.
[121] W. Luo, Y. Liu, F. Li, J. Huo, D. Zhao, J. Zhu, S. Guo, *Appl. Surf. Sci.* **2020**, *523*, 146387.
[122] Z. Lu, Y. Zhai, N. Wang, Y. Zhang, P. Xue, M. Guo, B. Tang, D. Huang, W. Wang, Z. Bai, S. Dou, *Chem. Eng. J.* **2020**, *380*, 122455.
[123] Y. Li, H. Wang, L. Wang, Z. Mao, R. Wang, B. He, Y. Gong, X. Hu, *Small* **2019**, *15*, 1804539.
[124] J.-S. Park, Y. J. Hong, J. H. Kim, Y. C. Kang, *J. Power Sources* **2020**, *461*, 228115.
[125] S. Ru, X. Wang, G. Ma, J. Tan, H. Xiao, Z. Ai, *Sustain. Energy Fuels* **2020**, *4*, 3477.
[126] Q. Ma, G. Du, W. Zhong, W. Du, S. Bao, M. Xu, C. Li, *J. Colloid Interface Sci.* **2020**, *578*, 710.
[127] S. Deng, Y. Zhang, D. Xie, L. Yang, G. Wang, X. Zheng, J. Zhu, X. Wang, Y. Yu, G. Pan, X. Xia, J. Tu, *Nano Energy* **2019**, *58*, 355.
[128] H. Wu, X. Zhang, Q. Wu, Y. Han, X. Wu, P. Ji, M. Zhou, G. Diao, M. Chen, *Chem. Commun.* **2020**, *56*, 141.
[129] M. Salavati, T. Rabczuk, *Comput. Mater. Sci.* **2019**, *160*, 360.
[130] Y. Zhang, L. Zhang, T. Lv, P. K. Chu, K. Huo, *ChemSusChem* **2020**, 1114.
[131] Y. Xue, Q. Zhang, W. Wang, H. Cao, Q. Yang, L. Fu, *Adv. Energy Mater.* **2017**, *7*, 1602684.
[132] Z. Xiao, Z. Yang, L. Zhang, H. Pan, R. Wang, *ACS Nano* **2017**, *11*, 8488.
[133] K. Wang, B. Zheng, M. Mackinder, N. Baule, H. Qiao, H. Jin, T. Schuelke, Q. H. Fan, *Energy Storage Mater.* **2019**, *20*, 299.
[134] J. Wang, J. Wang, Y. Zhou, C. Hu, *Acta Mater.* **2008**, *56*, 1511.
[135] C. J. Zhang, S. J. Kim, M. Ghidiu, M.-Q. Zhao, M. W. Barsoum, V. Nicolosi, Y. Gogotsi, *Adv. Funct. Mater.* **2016**, *26*, 4143.
[136] S. Zhao, X. Meng, K. Zhu, F. Du, G. Chen, Y. Wei, Y. Gogotsi, Y. Gao, *Energy Storage Mater.* **2017**, *8*, 42.
[137] D. Wang, Z. Xu, Y. Lian, C. Ban, H. Zhang, *J. Colloid Interface Sci.* **2019**, *542*, 400.
[138] L. Ni, G. Yang, C. Sun, G. Niu, Z. Wu, C. Chen, X. Gong, C. Zhou, G. Zhao, J. Gu, W. Ji, X. Huo, M. Chen, G. Diao, *Mater. Today Energy* **2017**, *6*, 53.
[139] P. Zhai, J. Qin, L. Guo, N. Zhao, C. Shi, E.-Z. Liu, F. He, L. Ma, J. Li, C. He, *J. Mater. Chem. A* **2017**, *5*, 13052.
[140] X. Wu, C. Qian, X. Zhang, H. Wu, L. Bu, L. Xu, M. Chen, H. Yan, Y. Piao, G. Diao, *J. Mater. Sci.* **2020**, *55*, 14464.
[141] G. Du, Y. Xu, S. Zheng, H. Xue, H. Pang, *Small* **2019**, *15*, 1804600.
[142] K. Hwang, H. Sohn, S. Yoon, *J. Power Sources* **2018**, *378*, 225.
[143] X. Cheng, S. Qian, H. Yu, H. Zhu, Y. Xie, R. Zheng, T. Liu, M. Shui, J. Shu, *Energy Storage Mater.* **2019**, *16*, 400.
[144] X. Liu, H. Wang, S. Zhang, G. Liu, H. Xie, J. Ma, *Electrochim. Acta* **2018**, *292*, 759.
[145] W. Zhang, S. Bu, Q. Yuan, Q. Xu, M. Hu, *J. Mater. Chem. A* **2019**, *7*, 647.
[146] Y. Wang, X. Xiao, Q. Li, H. Pang, *Small* **2018**, *14*, 1802193.
[147] L. Xu, H. Zhao, M. Sun, B. Huang, J. Wang, J. Xia, N. Li, D. Yin, M. Luo, F. Luo, Y. Du, C. Yan, *Angew. Chemie Int. Ed.* **2019**, *58*, 11491.
[148] J. Li, C. Shu, C. Liu, X. Chen, A. Hu, J. Long, *Small* **2020**, *16*, 2001812.
[149] D. Dambournet, C. Legein, B. Morgan, M. Body, O. Borkiewicz, F. Fayon, V. Sarou-Kanian, J. Ma, P. Strasser, T. Koketsu, W. Xiankui, M. Heggen, *Angew. Chemie Int. Ed.* **2020**, anie. 202007983.
[150] X. Wen, C. Ma, C. Du, J. Liu, X. Zhang, D. Qu, Z. Tang, *Electrochim. Acta* **2015**, *186*, 58.
[151] C. Yang, S. Yu, Y. Ma, C. Lin, Z. Xu, H. Zhao, S. Wu, P. Zheng, Z.-Z. Zhu, J. Li, N. Wang, *J. Power Sources* **2017**, *360*, 470.
[152] Z. Yao, X. Xia, S. Zhang, C. Zhou, G. Pan, Q. Xiong, Y. Wang, X. Wang, J. Tu, *Energy Storage Mater.* **2020**, *25*, 555.
[153] J. Zhang, C. Du, Z. Dai, W. Chen, Y. Zheng, B. Li, Y. Zong, X. Wang, J. Zhu, Q. Yan, *ACS Nano* **2017**, *11*, 10599.
[154] Y. Pan, *Ceram. Int.* **2019**, *45*, 18315.
[155] D. Ji, L. Fan, L. Tao, Y. Sun, M. Li, G. Yang, T. Q. Tran, S. Ramakrishna, S. Guo, *Angew. Chemie Int. Ed.* **2019**, *58*, 13840.
[156] W. Zhu, B. Zou, C. Zhang, D. H. L. Ng, S. A. El-Khodary, X. Liu, G. Li, J. Qiu, Y. Zhao, S. Yang, J. Lian, H. Li, *Adv. Mater. Interfaces* **2020**, *2000705*, 2000705.
[157] L. She, Q. Li, F. Zhang, L. Kang, X. He, J. Sun, Z. Lei, Z.-H. Liu, *J. Power Sources* **2020**, *451*, 227744.
[158] H. Yu, L. Xu, H. Wang, H. Jiang, C. Li, *Electrochim. Acta* **2019**, *295*, 829.
[159] H. Ding, J. Wang, L. Fan, Z. Liu, X. Jia, X. Yu, B. Lu, *Chem. Eng. J.* **2020**, *395*, 125147.
[160] L. Wang, X. Bi, S. Yang, *J. Mater. Chem. A* **2018**, *6*, 6225.
[161] P. Huang, M. Huang, H. Hu, Y. Zhong, C. Lai, S. Chou, *J. Mater. Chem. A* **2019**, *7*, 26513.
[162] C.-L. Ban, Z. Xu, D. Wang, Z. Liu, H. Zhang, *ACS Sustain. Chem. Eng.* **2019**, *7*, 10742.
[163] M. Zheng, Y. Chi, Q. Hu, H. Tang, X. Jiang, L. Zhang, S. Zhang, H. Pang, Q. Xu, *J. Mater. Chem. A* **2019**, *7*, 17204.
[164] J. Hu, J. Li, K. Wang, H. Xia, *Electrochim. Acta* **2020**, *331*, 135364.
[165] J. Y. Cheong, D. Y. Youn, C. Kim, J.-W. Jung, A. F. Ogata, J. G. Bae, I.-D. Kim, *Electrochim. Acta* **2018**, *269*, 388.
[166] Z. Chen, X. Cheng, W. Ye, R. Zheng, H. Zhu, H. Yu, N. Long, M. Shui, J. Shu, *Chem. Eng. J.* **2019**, *366*, 246.
[167] Y. Li, R. Zheng, H. Yu, X. Cheng, T. Liu, N. Peng, J. Zhang, M. Shui, J. Shu, *Electrochim. Acta* **2019**, *299*, 894.

[168] R. Zheng, S. Qian, X. Cheng, H. Yu, N. Peng, T. Liu, J. Zhang, M. Xia, H. Zhu, J. Shu, *Nano Energy* **2019**, *58*, 399.
[169] S. Lou, X. Cheng, Y. Zhao, A. Lushington, J. Gao, Q. Li, P. Zuo, B. Wang, Y. Gao, Y. Ma, C. Du, G. Yin, X. Sun, *Nano Energy* **2017**, *34*, 15.
[170] Y. Yuan, H. Yu, X. Cheng, R. Zheng, T. Liu, N. Peng, N. Long, M. Shui, J. Shu, *Chem. Eng. J.* **2019**, *374*, 937.
[171] W. L. Wang, B.-Y. Oh, J.-Y. Park, H. Ki, J. Jang, G.-Y. Lee, H.-B. Gu, M.-H. Ham, *J. Power Sources* **2015**, *300*, 272.
[172] T. Wang, T. Ma, T. Ge, S. Shi, H. Ji, W. Li, G. Yang, *J. Alloys Compd.* **2018**, *750*, 428.
[173] W. Ye, H. Yu, X. Cheng, H. Zhu, R. Zheng, T. Liu, N. Long, M. Shui, J. Shu, *ACS Appl. Energy Mater.* **2019**, *2*, 2672.
[174] X. Zhu, J. Xu, Y. Luo, Q. Fu, G. Liang, L. Luo, Y. Chen, C. Lin, X. S. Zhao, *J. Mater. Chem. A* **2019**, *7*, 6522.
[175] F. Ran, X. Cheng, H. Yu, R. Zheng, T. Liu, X. Li, N. Ren, M. Shui, J. Shu, *Electrochim. Acta* **2018**, *282*, 634.
[176] X. Zhu, Q. Fu, L. Tang, C. Lin, J. Xu, G. Liang, R. Li, L. Luo, Y. Chen, *ACS Appl. Mater. Interfaces* **2018**, *10*, 23711.
[177] C. Yang, Y. Zhang, F. Lv, C. Lin, Y. Liu, K. Wang, J. Feng, X. Wang, Y. Chen, J. Li, S. Guo, *J. Mater. Chem. A* **2017**, *5*, 22297.
[178] H. Nakayama, M. Nose, S. Nakanishi, H. Iba, *J. Power Sources* **2015**, *287*, 158.
[179] M. A. Reddy, U. V. Varadaraju, *Chem. Mater.* **2008**, *20*, 4557.
[180] K. J. Griffith, C. P. Grey, *Chem. Mater.* **2020**, *32*, 3860.

Yue Lian majored in chemistry. He is currently working toward a Ph.D. degree at the School of Chemistry and Chemical Engineering, Yangzhou University. His research direction concentrates on electrochemical energy storage.

Huaihao Zhang, a professor in the School of Chemistry and Chemical Engineering, Yangzhou University, received his Ph.D. degree from China Petroleum University in 2007. His major research interests focus on electrochemical energy storage, porous carbon materials, and chemical separation.

